Environmental and Chemical Investigation of Mortar of Termite Nests at Hada Al-Sham, Saudi Arabia for Biomimicry of Ecofriendly Constructions: A New Construction Theory

Sherif S. Hindi ,* and Khalid A. Asiry

*Corresponding author: shindi@kau.edu.sa

DOI: 10.15376/biores.20.2.4495-4540

GRAPHICAL ABSTRACT

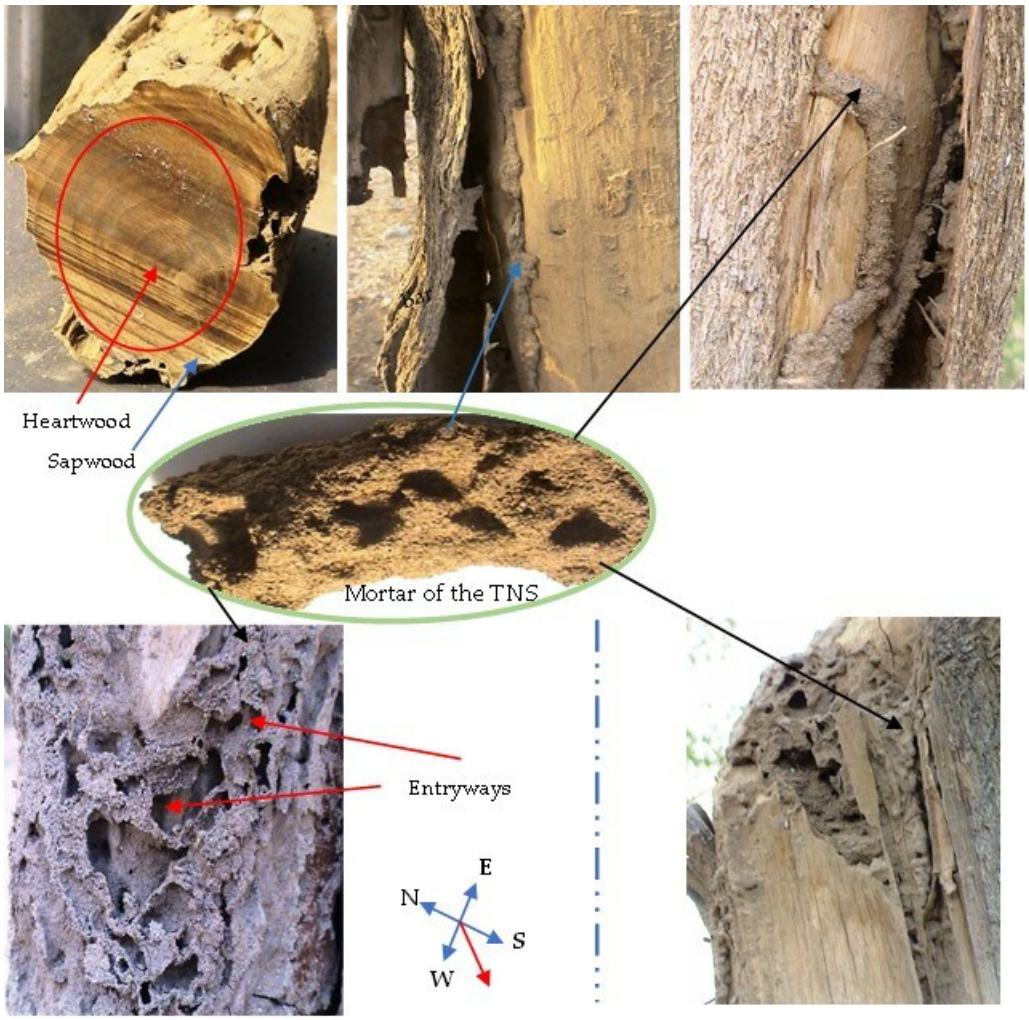

Environmental and Chemical Investigation of Mortar of Termite Nests at Hada Al-Sham, Saudi Arabia for Biomimicry of Ecofriendly Constructions: A New Construction Theory

Sherif S. Hindi ,* and Khalid A. Asiry

Nests made by the Najdian termite, *Microtermes najdensis*, were studied. The climate, soil, intact wood, and nest wall were investigated. The entryways of the termite nests were located at the southwest direction, which promotes better ventilation. The internal temperature (IT) was warmer than the outer temperature (OT) during cold days, while it was cooler than the hottest OT on hot days, and *vice versa*. The IT had more constancy than the OT. Moreover, the IT trended toward the upper OT's limit, indicating that termites prefer the hotter atmospheres. Lignin is the prominent tracer of the organic matter used as a binder for the nest wall due to its gluability and resistance to enzymatic or fungal degradation. Features resembling microcrystalline cellulose (MCC) and nanocrystalline cellulose (NCC) were discovered for the first time in the nest mortar reinforcing Klason lignin. Their presence was attributed to enzymatic hydrolysis by the termites and/or their accompanying fungal community. The gross heat of combustion (GHCs) of the intact wood and nest wall were studied. Finally, a theory illustrating the fabrication of termite nests was postulated.

DOI: 10.15376/biores.20.2.4495-4540

Keywords: Termite; Thermoregulator; Nest mortar; Lignin; Microcrystalline cellulose; Nanocrystalline cellulose

*Contact information: Department of Agriculture, Faculty of Environmental Sciences, King Abdulaziz University (KAU), Jeddah 21589, Saudi Arabia; *Corresponding author: shindi@kau.edu.sa*

INTRODUCTION

Many genera and species of termites have been brought from other countries inside shipments of wood and lumber, making them endemic permanent inhabitants (Gay 1967). According to its genealogy, termite colonies live in enclosed nests that are either subterranean (underground nests), arboreal (nests associated with trees), or epigeal (soil mounds) as described by Li and Greening (2022). The effect of three main ecological factors – vegetation, rainfall and topography – on the distribution and abundance of five termite genera commonly found in Saudi Arabia has been studied. Five genera include *Anacanthotermes*, *Psammotermes*, *Microcerotermes*, *Amitermes*, and *Microtermes*. Apart from termites of the genus *Microtermes*, those of the remaining 4 genera seem to have almost similar requirements. They prefer open scrubs (regions containing herbs and shrubs), moderate mean annual rainfall (ranging between 50 and 150 mm), and are more abundant in plateau areas. On the contrary, *Microtermes* has 50% of its sampling sites located in open scrubs and about 40% in large trees/grass areas. The genus prefers

relatively higher mean annual rainfall (ranging between 250 and 500 mm) and are more abundant in plains (Badawi *et al.* 1986; Sharaf *et al.* 2021).

Numerous termite species are found in rural, urban, and suburban habitats (Reginaldo and Dianese 2001). The subterranean termites have been classified ecologically into four groups, namely drywood, damp wood, harvester, and subterranean termites (Al-Ghamdi *et al.* 2009). *Microtermes najdensis* Harris (Isopetra, Termitidae), a small underground termite, was discovered at Hada Al-Sham (Al-Ghamdi *et al.* 2009; Faragalla *et al.* 2013). In addition, termites belonging to the Kalotermitidae, Hodotermitidae, Rhinotermitidae, and Termitidae families were discovered in Saudi Arabia. The first three are lower developed families, whereas the fourth one is a highly developed family termed as Termitidae (Faragalla *et al.* 2013). The annual losses due to their heavy infestations in human life have reached a great level, leading to applying prophylactic and preventive methods (Koehler *et al.* 1998; Su and Scheffrahn 1998; Faragalla *et al.* 2013).

Termite nests have diverse and complicated structures that provide tight enclosures that protect the colonies from predators (Jost 2020). Their intricate architecture have been fascinating and inspirational for societal collective building, or a scientific study objective (Jost 2020). These structures have been used as exemplary of bioinspired designs, in buildings, for air-conditioning control (adjusting internal temperature and relative humidity), balancing each of energy and gas- exchanging between inner and outer nest' system (Turner and Soar 2008; Jost 2020). Termite nests' constructions are often quite species-dependent, meaning that different species in the same habitat can create nests of varying firmness. The chemical structure of their saliva and faecal material, as well as the clay/sand ratio, influence nest solidity (Jost 2020).

The main source of food for termites is wood, grass, leaves, humus, animal excrement from herbivores, and plant-based goods including paper, cardboard, and cotton (Keegstra *et al*. 1973; Wood and Sands 1978; Eriksson 1993; Li and Greening 2022). It makes sense that termites require three things to survive: food, water, and air. For nutrition, Ulyshen (2014) reported that some termites' groups depend on nutrition produced from decayed wood, which is facilitated by numerous developing fungi. The amazing and extraordinary behavior of these termites' species is their transferring fungal spores by unique structures on their bodies called mycangia (Ulyshen 2014). After that, they spread these spores within their nests' floor in order that the spores will be able to continue their growth cycle (Collins 1981; Darlington 2000). Furthermore, termites get water from their food sources (dry wood) or from damp, dead, rotten wood, respectively (Krishna 1989). Contrarily, subterranean termites are compelled to contact soil to fulfill their thirst for water and moisture. As a result, subterranean termites have evolved into the most costly and damaging to human property, woodwork, stored goods, buildings, and wooden infrastructure (Su and Scheffrahn 1998).

Due to their stealthy eating habits, subterranean termites are nearly impossible to detect unless their galleries, such as earth tubes and tunnels, are rendered visible together with a significant infestation of wood that has been hollowed out and filled with fine earth particles (Arshad 1981; Al-Ghamdi *et al*. 2009; Chouvenc and Su 2012).

The diet of termites is basically rich in cellulose and hemicelluloses as well as lignin or its derivatives (Varma *et al.* 1994; Donovan *et al*. 2000; Ptáček *et al*. 2013). Termites may digest lignocellulosic materials due to the collaboration of their own enzymes and foreign enzymes from microbes. Termites can be divided into six feeding categories based on their preferred food: wood, dry wood, wood and litter, soil, fungus, and grass. The termite stomach supports highly specialized cellulolytic and hemicellulolytic microbes.

Certain xylophagous termites form an unusual nutritional relationship with their hindgut protozoa. Furthermore, termites and cockroaches' foreguts and midguts, as well as their salivary glands, showed cellulase activity, according to Slaytor (1992). These areas are the typical sites where digestive enzymes are secreted, and there are no or very few microorganisms present. Therefore, there is no proof that termite cellulose digestion is mediated by bacteria.

Since cellulose is reinforced by lignin in the higher plants' cell walls (Jost 2020), preventing its bio-digestion, accordingly, the symbiotic fungi start with disturbing lignin to ensure accessibility for the termites' own cellulase (Grassé and Noirot 1958; Hyodo *et al*. 2000; Ptáček *et al*. 2013). The efficiency degrading and consuming cellulose and hemicelluloses from wood by termites using wood was estimated to range from 59 to 99%. Acetate, CO_2, and H_2 are produced when protozoa or a termite's own cellulolytic enzymes directly ferment cellulose under anaerobic conditions. The acetate is subsequently absorbed by the termites, who utilize it as their primary source of oxidizable energy (Slaytor 1992; Varma *et al.* 1994).

Concerning nest constructing materials, they are prepared mainly by the termites themselves. The materials also can be woody-degraded residues, including Klason lignin (the main binder) and organic matter residues, as well as the earth-based materials collected and transported by these insects (Badawi *et al*. 1982, 1986). For the earth materials, sand, silt, loam, clay, and loose forms of soil with various levels of organic matter contents were all observed to be types of soil that the termites themselves used to build their nests (Badawi *et al*. 1982). Similar to the way that lignin provides mechanical support to plant vasculature, its polymeric network also has been reported to reinforce the skeleton of termites' wall nest, which was reported to serve as a barrier against microbe attack and a water-tight seal (Varma *et al.* 1994). Several researchers have studied termites' feces from the point of view of predicting the activity of termite colonies and/or utilizing the output information as a trial to differentiate the termite species as a taxonomical purpose (Fajar *et al.* 2020).

White rot fungi can degrade lignin aerobically inside their cells by oxidative enzymes (ligninase peroxidase, manganese peroxidase, and laccases) faster than other organisms (Tuomela *et al*. 2000). According to the lignin degradation theory, symbiotic fungi can degrade lignin, allowing termites' own cellulase to consume cellulose (Grassé and Noirot 1958; Hyodo *et al*. 2000). The absence of any known lignin-degrading bacteria in termite guts and the lack of a known location for lignin degradation both lend credence to the theory (Klemm *et al.* 2005). Since lignin's polyphenolic structure is more resistant than that of other wood polymers, it has long been thought to be a significant source of stable carbon in soils (Rasse *et al*. 2006). In addition, turnover studies of lignin have revealed that large allocations of it were decomposed within a year of when embedded in soils (Rasse *et al*. 2006). Furthermore, the lignin content in older nests was only half that of younger nests. These results are in basic agreement with those indicated by Rückamp *et al*. (2011).

Termite nests are often rich in organic material. Given that most termite species can't degrade lignin, which was found to be 15 times more abundant at 10 cm depth of the reference soils, lignin might be a useful tracer of the organic matter incorporated into termite nests and released into nest surroundings (Rückamp *et al*. 2011). Elevated lignin contents were found at 60 cm distance from the nest border as well as up to 60 cm soil depth beneath the nests. The lignin content in older nests was only half that of younger nests, and the influence on the nest surroundings was less prominent. Moreover, the savanna termite *C. silvestrii* has been found to enrich lignin in its earth mounds, but that

only a minor part enters the soil-protected lignin fraction when nests decay, as most of the lignin is lost during nest aging (Rückamp *et al*. 2011).

Higher lignin content was discovered 60 cm from the edge of the nest and up to 60 cm into the soil beneath the nests. Older nests had lignin contents that were about half as high as those of younger nests, and their influence on the area around the nest was less pronounced. Furthermore, the savanna termite *C. silvestrii* enriched lignin in its earth mounds; however, only a little portion of this lignin enters the soil-protected lignin fraction when nests degrade because most of the lignin is lost during nest aging (Rückamp *et al*. 2011).

The crystallinity of cellulose is defined as the ratio of the amount of crystalline cellulose to the total amount of sample material, including crystalline and amorphous parts. The CCs comprise different types of cellulose-based materials. The following terms have become well established as isolated products for research and industry: microcrystalline cellulose (MCC), nanocrystalline cellulose (NCC), cellulose nanorods (CNR), cellulose nanowhiskers (CNW), cellulose microfibrils (CMF), and cellulose nanofibrils (CNF) (Hindi 2017a-d, 2018 and 2020-2022 a,b). Some of the same terms will be used in this article to refer to features that have been observed with natural termite nests.

The MCC is pure partially depolymerized cellulose synthesized from α-cellulose precursor. The MCC can be synthesized by different processes such as reactive extrusion, steam explosion, and hydrolysis. The later process can be done using mineral acids such as H_2SO, HCl, HBr, ionic liquids and bioenzymes, synthetically or naturally by micro-organisms. The role of these reagents is to destroy the amorphous regions remaining in the crystalline domains (Hindi 2017b). Because of its exceptional dry binding capabilities, MCC is a beneficial ingredient in pharmaceutical applications as a tablet binder, as well as in food and cosmetic applications as an anticaking, thickener, texturizer, emulsifier, and bulking agent (Hindi 2017b). Moreover, due to its high strength, flexibility, and aspect ratio, MCC is also used in paints, paper and nonwoven textiles, oil field services, medicine, and composites.

The NCC has been defined as a nanoscale form of cellulose that has at least one dimension less than 100 nanometers in size (Hindi 2017a). The size, dimensions, and shape of NCCs are determined by the type of cellulose supply as well as the hydrolysis conditions such as duration, temperature, ultrasonic treatment, and material purity (Hindi 2017 d). In addition, regarding its high thermal stability, NCC can be regarded as a high potential filler for industrial nanocomposite applications. The charged NCCs' particles create an anisotropic liquid crystalline phase above a certain concentration (Hindi 2017 c).

Many farmers and customers are suffering from infestation of their timber trees by termites. Accordingly, utilization of such infected woody raw materials as a heat sink can reduce economic losses arising from the termites' infection. According to reports, sustainability in energy recovery from biomass is becoming more appealing because biomass emits no new greenhouse gases into the environment (Hindi 2011, 2012). Timber trees' potential as plantation species is becoming more widely acknowledged in Saudi Arabia, particularly for fast-growing species. In addition to their value as windbreaks and shelterbelts, wood is used as a source of energy through direct burning, particularly in rural locations, villages, and during Muslim pilgrimage at Mena and Araft camps, to provide heat for cooking and other traditional uses. Firewood and charcoal are commercially marketed in various locations of Saudi Arabia at large public markets as well as traditional stores. The widespread use of firewood in Saudi Arabia stems from Saudi customs and a preference for Arabic cooking flavors (Hindi 2012**)**. Lignocellulosic species were argued

to be better suited as fuelwood species due to their high-density wood, low ash content, and low nitrogen content. The gross heat of combustion (GHC) of wood is an important property that determines the suitability of such wood species for renewable energy supply. There was found to be a strong relationship between the GHCs of woody materials and their contents of lignin, fixed carbon, and volatile matter contents (Hindi 2011, 2012).

In Saudi Arabia, especially the western region, systematic field investigations are available only for some metropolitan areas where grave damage has occurred on wood used in construction or infrastructure or in heavy infestation on agricultural crops.

Since termite nests are less well studied than those of many pests such as ants, social wasps, and social bees, particularly honeybees and stingless bees, this study was focused on studying these nests. Furthermore, several scientists investigated the construction and composition of termite nests referring only to their macro- and micro-scaled materials including lignin, sand, clay and organic matter contents, but no one detected the incorporation of crystalline celluloses (MCC and NCC) within the skeleton of termite nests. Accordingly, this study was initiated to study:

1) The most infected tree species, comparing their susceptibility to infection by the small Najdian termite, *Microtermes najdensis*.
2) The structures of termite nests as exemplary of bioinspired buildings' designs for enhancing internal atmosphere (temperature, humidity and ventilation) of buildings.
3) The mortar composite blend (soil, lignin, calcium carbonate, MCC, NCC) used for constructing the termite nest.
4) The mechanical properties of the nest skeleton to determine its suitability for particleboard products and studying the GHC of the partially-infected wood to determine its suitability as renewable energy resources.
5) The suitability of the partially-infected wood as a renewable energy resource.

EXPERIMENTAL

Management Plan

Images related to termite nest and related environmental features are provided in the Appendix. Features including the termites (Fig. A1), their surrounding's elements (Fig. A2), namely atmosphere (Fig. A2a1), soil (Fig. A2a2), the tree species (Fig. A2a3), and their nest wall (Fig. A2a4) are presented. In addition, the termite system characterization was shown at Fig. A2B, namely air temperature (Fig. A2b1), soil in open field and the nest wall (Fig. A2b2), intact wood (Fig. A2b3), nest wall (Fig. A2b4).

Under suitable climatic conditions (temperature and relative humidity), the termites carry out their daily activities to provide food and shelter for themselves. The termites are able to digest lignocellulosic materials such as wood and degrade it. Bio-enzymes excreted by fungus are cultivated in the nest's gardens, where they influence the nature of organics such as faecal materials, lignin, and cellulosic particles. The termites also transport soil/clay particles into their nests within the infected trees and mix these ground particles with the organics, lignin, and cellulosic particles, wetting this blend with their saliva.

Studying the Termite System

The termite system investigated in the present investigation was considered to be constituted of four elements, namely of atmosphere, soil, tree species, and nest wall (Fig. A2).

The experiment was conducted at the Agriculture Research Station (ARS) of King Abdulaziz University located at Hada Al-Sham, northeast of Jeddah (21° 48′ 3″ N, 39° 43′ 25″ E), Saudi Arabia during the period extending from 01 October 2019 to 30 August 2020.

Atmosphere

The dominant air temperature data of the study area were collected from the local meteorology station's saved database that was measured at a constant level of two meters above ground level.

Moreover, within termite nests, the internal atmosphere measurements were limited to air temperature recording. For this task, continuous temperature measurements were taken daily, at specified times in six hours intervals throughout the recording period (11 months) for each of the infected trunk of *Ziziphus spina-christi* (01 October 2019-31 August 2020). The starting record was 12 am on 1 October 2019. The measurements were recorded manually using digital thermometers with chromel-alumel thermocouple probes (type K with an error of ± 1 °C). Each thermometer's probe was introduced deeply inside the termite nest passing through a naturally formed tunnel spreading at the southwest direction. Since the pathways' galleries of the nest are not straight, an electric drill with a long steel drill bit (size 0.25 inch; maximum drilling depth 10 inches) was used to engrave a straight pathway for entrance the thermometer probe into the nest. It is worth mentioning that the artificial facial opening of the nest done by the drill was closed by a binding paste such as epoxy paste, or honeybees wax to prevent changing the meteorological parameters within the nest as well as preventing predators from entering the nest. The starting record was about 12 AM.

Soil

The soil properties in the open field were determined as well as the minerals incorporated in the mortar that termites used during constructing their nests. In order to prevent any termite infestation, the reference soil sites were chosen to be at least 5 m away from termite nests and did not appear to have been influenced by termites. Each sampling location had three soil transects drilled from the site's center to its four cardinal points. For each transect, samples were collected at soil depths of 10, 30, and 60 cm at a constant width of 40 cm. The soil samples present at the horizon borders were avoided, and the accurate samples were about 5 cm above or below the referred borders according to Rückamp *et al.* (2011). Four random soil samples from the surface layer (0 to 30 cm depth) were collected just beneath each infected tree chosen for this study. The collected soil samples were air dried, sieved, and analyzed for different physical and chemical properties. The contents of clay, silt and sand, texture class, bulk density, air porosity, organic matter content (organics), EC, and pH were determined according to Asiry *et al*. (2022) and Wang *et al*. (2023).

While EC offers an operationally defined assessment of a soil's salinity, pH is an operationally defined measure of the H+ ions that are active in soil solution that are important indicators of soil health (Balkhair *et al*. 2016; Elfaki *et al*. 2016). Their water-based measurements were performed in 1:1 with a 1:1 soil-to-deionized water ratio so that comparisons of pH readings are done on an equivalent basis (Kome *et al*. 2018).

Furthermore, total organic matter content (organics) of the soil particles collected from the open field just beneath the six infected tree species as well as those particles presented at the nest wall mortar was done by applying loss on ignition (L_oI) method, which is known to be one of the most widely used methods for this task (Ptáček *et al*. 2013; Hoogsteen 2015; FernandesIldeu 2015). The L_oI method was done at 450 °C during 5 h and at 600 °C during 6 h; and by the dry combustion method (Hoogsteen *et al.* 2015) using tube furnace (Carbolite). Since many factors may influence accuracy of this determination process such as furnace type, sample mass, duration, and temperature of ignition and clay content of samples (Ptáček *et al*. 2013; Hoogsteen *et al.* 2015), all these factors were standardized for all the tests. Concerning total minerals content (minerals) in soil (open field) after thermal elimination of total organics, the organic carbon (O. carbon) was measured with an elemental analyzer (NA 2000, Fisons Instruments, Rodano, Milan, Italy). Subsequently, the minerals of some selected soil samples were characterized by X-ray diffraction (PW 1130, Philips, Almelo. The Netherlands).

Moreover, for particle size distribution of soil, each of oven-dried soil particles collected from the open field just beneath the six infected tree species was mechanically sieved at room temperature in a 100-g batch and separated into four sieved particle size fractions, namely less than 125 µm, 125 to 300 µm, 300 to 425 µm, and more than 425 µm. The four particle gradients were determined as a percentage based on their original weight.

The tree species

The intact wood samples isolated from the six infected tree species as well as their lignocellulosic components (lignin, MCC, NCC) isolated from the nest wall mortar were characterized.

The most susceptible tree species to infection by Najdian termite, *Microtermes najdensis* located at Hada Al-Sham village, KSA were chosen from the enormous species habituating and cultivated in the KAU farm to study the termite infection as well as their susceptibility to the termite attack. These species were *Tamarix aphylla* (L.) H.Karst. (Family: Tamaricaceae), *Pithecellobium dulce* (Roxb.) Benth. (Family: Fabaceae), *Ziziphus spina-christi* (L.) Desf. (Famiy: Rhamnaceae), *Leucaena leucocephala* (Lam.) de Wit (Famiy: Fabaceae), *Ficus infectoria* Roxb. (Famiy: Moraceae), and *Phoenix dactylifera* L. (Family: Arecaceae). Three trees were selected from each species representing three replicates. Both the first and the latest genus (*Tamarix* and *Phoenix*) are native to Saudi Arabia, while the other four genera were not.

To determine the wood's qualities, a diametric disc was sawn from each selected tree at a height of 0.6 m (approximately 30 cm thick) with a defined diameter that differed among trees due to variation in their botanical nature (branching pattern) and age. However, their diameters were graded from 40 cm (for *Z. spina-christi* and *L. leucocephala*, respectively) continuing to 50 cm (for *T. aphylla* and *P. dactylifera* respectively) up to about 60 cm (for *P. dulce* and *F. infectoria*, respectively). The isolated discs were used to determine the wood's qualities, as shown in Fig. A3.

One bolt (approximately 1.8 cm tangentially and 30 cm long) was sliced longitudinally after the pith was isolated. Each inner- and outer-wood zone of each bolt had a diametric strip (nominal 1.8 cm tangentially and radially, and 30 cm longitudinally) removed. Accordingly, each bolt yielded two diametric strips. As a result, the removed strip was afterwards crosscut into four imperfection-free cubic samples as shown in Fig. A3.

The remaining volume of the wood disc, excluding inner or outer wood zones, were separately converted into meal. Based on the standard methods for determining wood quality, wood meal was screened using various standard sieves and specified for the determinations of extractives, lignin, holocelluloses, and ash of the six lignocellulosic materials.

Three samples were randomly selected from each tree (a total of 9 samples of the three trees specified for each species) for each determination. For the six wood resources that were employed for each determination, 54 samples were accordingly specified. Concerning the characterization, wood properties were considered were prepared (Fig. A3), using the standard and technical methods (Fig. A4), and their values were calculated as shown in Table A1.

The nest wall

It was assumed that the majority of nests were built around mid 2019/2020. In order to select the infested tree species and determine the termite nests' locations within the trees, there was intensive monitoring of all lands within the ARS. The nests included numerous passageways and galleries with dense walls made primarily of organic residues arisen essentially from the infested woody trees themselves, as well as earth material transferred from beneath the infested trees-bearing the termite nests (Appendix). Due to the majority of their apertures being on the western side, the nests appeared warmer than the outer surrounding climate. For sampling, three replicates of each nest as well as reference soils were chosen according to Al-Ghamdi *et al*. (2009) and Faragalla *et al* (2013).

Termite nests were sampled at about 50 cm above the ground level. At each location, five 100 cm^3-cores were used for the sampling process. Every sample was promptly air dried after collection. Regarding physical and chemical characterization, the following properties were considered for the wall nest. After selecting the six tree species, wood samples were prepared for the intact wood, and the nest wall as illustrated in Figs. A1-A5 and Table A1.

Wood Characterization

Specific gravity (SG)

The SGs of the intact wood, as well as the nest wall samples were determined by using Pycnometric displacement of water based on oven-dry weight and saturated volume. Five defect-free samples (2.5 cm radially and tangentially and 2 cm longitudinally each) were used from each tree (15 samples of each species). Accordingly, 90 samples were specified for the six tree species used. The green samples assigned for this test were accurately re-saturated by water under vacuum and the saturated volume was measured by Pycnometric displacement of water. The SG was calculated based on oven-dry weight and saturated volume as presented at Table A1.

Extractives of the intact wood

The extractives of the Intact Wood were determined according to the ASTM (1989 b). Each sample assigned for extractives content determination was about one gram of an air-dried wood meal that has been ground to pass through a No. 60 (250 urn) sieve and be retained on a No. 80 (180 um) sieve. The samples were extracted in a Soxhlet apparatus with ethanol-benzene mixture (in ta ratio of 1:2) for 4 hours, followed by extraction with 95% ethanol for 4 hours, then extraction with a hot deionized water for 3 hours with changing of water every one hour. The extracted sample was oven-dried to a constant

weight at 103 ± 2°C, and the extractives were calculated using the formula presented at Table A1.

Holocelluloses of the intact wood

The combination of hemicelluloses and alpha cellulose makes up the holocelluloses of wood (Trilokesh and Uppuluri 2019). According to the methodology outlined by Wise *et al.* (1946) and Hindi *et al* (2011), it was determined as follows: A 5 wt% fiber solution was made and combined with 0.75 g of sodium chlorite and 0.5 mL of glacial acetic acid. The temperature was held at 75 °C for one hour while the flask was top sealed to prevent the loss of gas generated during the reaction process. The chemical reagents were changed twice. The holocelluloses of wood was calculated as presented at Table A1.

Lignin content

The lignin content of each of intact wood as well as the nest wall samples was determined according to ASTM (1989c), Hindi *et al* (2011), and Gaudenzi *et al.* (2023). The diluted sulfuric acid solution (72%) was used to hydrolyze the extractives-free wood sample at 30 °C for 4 h. The sample was secondarily hydrolyzed after being primarily hydrolyzed for 2 h at a concentration of 3 % (wt/wt). Whatman filter paper No. 44 was used to filter the material, which was then dried by air, oven, and weight. The lignin was determined as clear in Table A1.

Ash of the intact wood

The ASTM (1989 d) was used to determine the ash of the intact Wood. The wood meal samples weighing about 2 g each that had been ground to pass through a No. 40 (425 um) sieve were gathered. Each sample was put into a porcelain crucible, dried in an oven at 103 ± 2 °C to a constant weight, and then weighed. In a tube furnace, the exposed crucible containing the sample was lit at 600 °C until all the carbon was burned off. It was then weighed after cooling in the desiccator. Up until the weight after cooling is constant to within 0.2 mg, the heating was repeated at 30-min intervals. Based on the weight of the oven-dry wood meal, the proportion of residual containing ash was estimated (Table A1).

The gross heat of combustion (GHC)

The GHCs of the intact wood as well as the nest wall samples were determined. This was done after preparing the GHC's specimens as shown in Fig. A3. The GHC of each of the intact wood and the wall nest was determined using an adiabatic oxygen bomb calorimeter, Parr 1341, in accordance with the ASTM (1987), as well as the procedures stated by the Parr instruction manual as explained by Fig. A5. The intact wood samples were prepared according to the flowchart presented in Fig. 1. Using a pellet press, model Parr 2811, each sample (0.8 g) designated for measuring GHC was formed into a pellet. The samples were dried in an oven and weighed. The calorimeter was calibrated using pellets of benzoic acid. Under carefully regulated circumstances, the sample was inserted into a metallic capsule and exploded within the oxygen bomb Parr 1108.

Using a mercury thermometer (Parr 1603), temperature observations were recorded before, during, and after combustion. On a moisture-free basis, the heat generated by a sample's combustion was estimated and converted into calories per grams. The estimates for the GHC included correction factors for the combustion of fusing wire and thermometer. On the other hand, because they are too minor to consider, correction factors for the generation of nitric and sulfuric acids were not included in these calculations

(Neenan 1979; Zachariah *et al.* 2020). These calculations with their corrections are clarified in Table A1 and Fig. A5.

Mechanical properties of the nest wall were examined to determine their suitability as a bioinspired composite material in building sectors, especially at rural villages and tourist regions. Each wall nest mass (see Fig. 7) was sectioned into slices and samples were extracted from each slice according to Zachariah *et al.* (2020).

The stress–strain behaviors of the wall nest collected from six infected tree species were measured using an Instron universal testing machine, model 1193, Instron Co., Ltd., London, UK, with a 200 N-load cell according to Guarino *et al.* (2007). The device with two metallic grips was installed to hold the test sample at both ends. The starting grip separation for all samples was 50 mm, and the upper grip was extended at a constant rate of 50 mm per min, while the lower grip remained stationary. An automatic speed controller was fitted to the electrically powered machine to maintain the upper grip's speed. The ambient temperature was used for all measurements. From the plot of stress–strain curves, the mechanical properties, namely, ultimate tensile strength (UCS) in MPa, modulus of elasticity (MoE) in MPa, and deformation at failure (EaF) as a percentage, were calculated (Table A1).

The ultimate compressive strength (UCS) of the wall nest shows its maximum allowable compressive stress. The UCS property was calculated by dividing the maximum load causing the failure of the wall nest by the cross-sectional area of the specimen, as explained in Table A1.

The modulus of elasticity (MoE) is a reliable indicator of the wall nest' stiffness. The MoE was computed by dividing the stress at yield by length of the wall nest' specimen at yield, as expressed in Table A1.

Concerning the deformation at failure (DaF) it was calculated by dividing the deformation at failure of the wall nest specimen by the initial gauge length, as shown in Table A1.

An attempt to detect the presence of micro- and nanometric-scaled materials (matter resembling microcrystalline or nanocrystalline cellulose) synthesized by natural enzymatic hydrolysis was performed as a novel trial to interpret the nest endurance to violent weather conditions in such regions.

The "MCC" represents the micrometric-scaled polymeric materials detected in the nest wall, while the "NCC" is the famous nanoparticles assembly the nest wall that were discovered for the first time. MCCs and NCCs samples were assigned to XRD, FTIR, SEM and TEM investigations. For the XRD, FTIR, since their micrometric-scale samples must be a fine powdered form, they were ground in a ball mill to pass through a 100 mesh and be retained on a 120 mesh. For each of the MCC and NCC samples specified for SEM and TEM spectroscopic studies, a thin film of each individual solution was required for each characterization. This solution was prepared from each powder type that was completely dissolved in absolute ethanol by assistance of sonication.

Imaging using SEM and TEM techniques was used in the present investigation to confirm the presence of apparent micro- and nano-crystalline cellulose (MCC and NCC) in the constructed nests' wall.

SEM imaging was used to study the surface morphology and types of anatomical features in the tangential plane samples of leaflet tissue as well as the SCNCs. The samples were placed on the double side carbon tape on Al-stub and dried in air. Before examination, all samples were sputtered with a 15 nm thick gold layer (JEOL JFC- 1600 Auto Fine Coater) in a vacuum chamber. The samples were examined with a SEM Quanta FEG 450,

FEI, Amsterdam, Netherland. The microscope was operated at an accelerating voltage ranging from 5 to 20 kV (Hindi 2017c,d).

TEM characterization was examined by TEM (JEM-1011 JEOL, Japan). The suspension was sampled by using a capillary pipet and dropped onto the copper grid. After being dried for 3 min at ambient condition, filter paper was used to remove the excess liquid on the copper grid. The dye liquor of phosphotungstic acid was dropped and dyed for 2 min. The dried sample was prepared for observed. The operated voltage was at 100 kV (Hindi 2017 c).

FTIR spectroscopy was used to determine the chemical structure (functional groups) of the parent alpha as well as the cellulose-based products (MCC and NCC). Specimens were investigated by the FTIR using a Bruker Tensor 37 FTIR spectrophotometer. The samples were dried at 100 °C for 4 to 5 h, mixed with KBr in a ratio of 1:200 (w/w), and pressed under vacuum to form pellets. The FTIR-spectra of the samples were recorded in transmittance mode in the range of 4000 to 500 cm^{-1} (Hindi 2017c,d).

The X-ray powder diffraction (XRD) spectra of wood-based samples were used to study the crystallinity of the XRD-D_2 Phaser Bruker (USA). The generator was operated at 30 KV and 30 mA. The samples were exposed for a period of 3000 s using CuKa radiation with a wavelength of 0.15418 nm. All the experiments were performed in the reflection mode at a scan speed of 4° /min in steps of 0.05°. All samples were scanned within a 2θ=26° range from 4° to 30°. For estimating crystallinity index, individual crystalline peaks were first extracted by a curve-fitting process from the diffraction intensity profiles. The CI was calculated by dividing the diffractogram area of crystalline cellulose by the total area of the original diffractogram. The area under the curve was estimated by summing of adjacent trapezoids using Excel (Microsoft, USA), as indicated by Hindi (2017e).

Statistical Design and Analysis

A randomized complete block design (RCBD) with three replications was used in this study. Each of the six plant species was considered statistically as a separate block. Moreover, each block was repeated three times to enable calculation of the experimental error. Accordingly, three trees were used from each species. Differences between groups were examined with an analysis of variance (ANOVA), and the LSD0.05 test for comparing the mean values of each property examined. The significance level was set at $P < 0.05$. The ANOVA was conducted with SPSS 14.0 (SPSS Inc. 2005, Chicago, USA) as illustrated by El-Nakhlawy (2009).

RESULTS

Climate

Climate at Hada Al-Sham

Concerning the most important parameters dominant at Hada Al-Sham region collected from the local meteorological station, their mean values were presented at Table 1 and Fig. 1.

Table 1. Climate at Hada Al-Sham: Air Temperature (AT), Soil Temperature (ST), Income and Outcome Radiation for Each of Shortwave and Longwave, Wind speed (WS), Wind Direction (WD), Barometric Pressure (BP) during January 2021

Property	Height	Mean	Max	Min
Air temperature (°C) at:	2 m	24.69	33.29	14.56
	5 m	24.75	32.7	15.85
	10 m	22.63	63.91	-0.683
Soil temperature at 50 cm (°C)		28.79	31.37	27.93
Radiation wavelength	Income shortwave	33.79	143.3	-0.029
	Income longwave	6.26	41.76	-9.39
	Outcome shortwave	184.53	837	-6.451
	Outcome longwave	-42.579	-3.387	-84.1
Wind speed at 10 m, m/sec		2.38	11.66	0
Wind direction at 10 m, degrees		159.52	353.6	0.071
Barometric pressure, mbar		988.08	993	983

[1] N=1492.

Concerning the conditioning status within the termite nest, the internal temperature of the nest and the outer temperature (OT) of the surrounding atmosphere were monitored, measured, and plotted against time in six hours intervals during the period extended from October, 2018 up to the end of August 2020 as shown in Fig. 1.

The eleven months included for the temperature measurements were October 2019, November 2019, December 2019, January 2020, February 2020, March 2020, April 2020, May 2020, June 2020, July 2020, and August 2020 as shown in Fig. 1.

The obtained histograms matched the historical temperature data in which the minimal value of January is the coldest month, and the months from October to April are colder than the summer months.

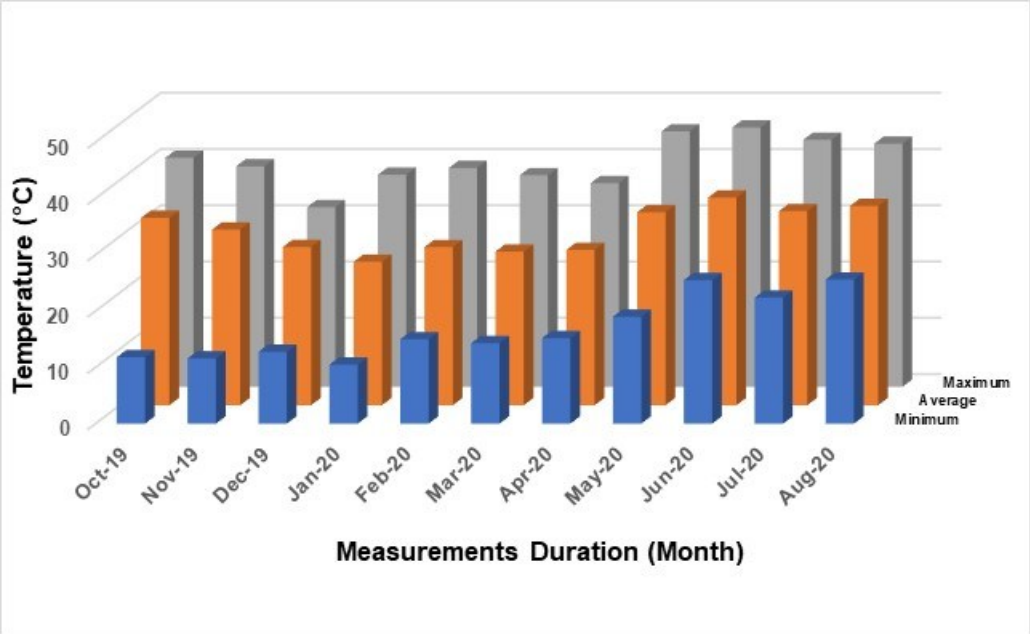

Fig. 1. Temperature parameters (minimum, average, maximum) of the interior within the termite nests engraved naturally within the infected trunk of *Ziziphus spina-christi* grown at Hada Al-Sham village.

As shown in Fig. 2, the IT was milder than those for their analogous values for the outer environment, namely outer temperature (OT). In summary, the IT was warmer than OT during cold durations, while it was colder than the hottest OT in hot days and vice versa (Korb and Linsenmair 2000; King *et al*. 2015). Moreover, the IT was exceeded more than its average level and towered higher temperatures.

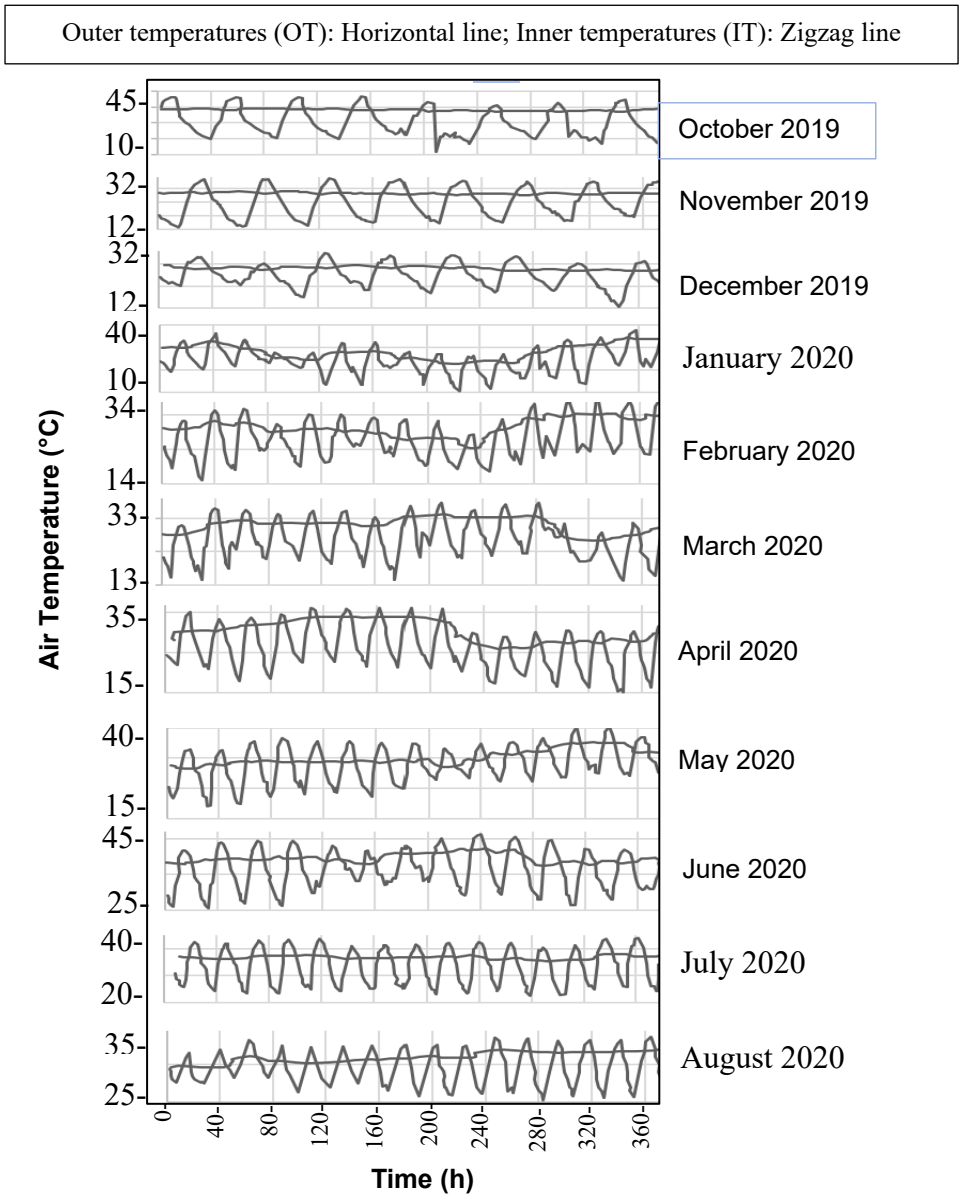

Fig. 2. Air Temperatures throughout eleven months within (IT) and outer (OT) of the termite nests engraved in the infected trunk of *Ziziphus spina-christi* grown at Hada Al-Sham village

Soil

Open field's soil (OFS)

The OFS collected just beneath the six infected tree species is shown at Table 2 for the most important chemical and physical properties. These properties were extended to cover the percentage contents of clay, silt and sand, texture class, bulk density, porosity, organic matter content (organics), EC, and pH (Asiry *et al*. 2022; Wang *et al*. 2023). It can

be seen from Table 2 that the sandy loam soils collected from the open field adjacent to the infected trees within the Agricultural Research Station of the KAU had a higher sand content (74.8%) than their contents of silt and clay (15.5% and 9.7%, respectively). Moreover, their mean values of bulk density, porosity, organic matter, electrical conductivity and pH were estimated to be 1.87 g/cm^3, 29.4 %, 0.65 %, 0.366 dS m^{-1} and having weak alkalinity of 7.7, respectively.

Table 2. Mean values of Physical and Chemical Analyses of the Virgin Soil Surrounding the Infected Sites that Would be Used by Termites to Construct their Nests

Variables	Mean Value *
Clay (%)	9.7 ± 0.251
Silt (%)	15.5 ± 0.316
Sand (%)	74.8 ± 2.854
Texture class	Sandy loam
Bulk density (g/cm^3)	1.87 ± 0.087
Porosity (%)	29.4 ± 1.634
Organic matter (%)	0.65 ± 0.087
EC (dS m^{-1})	4.06 ± 0.072
pH	7.70 ± 0.214

* Each value is an average of 5 samples ± standard deviation.

Electrical conductivity (EC) of soil

Figure 3a shows that EC of the soil particles used to construct the termite nest was found to be higher than that for the parent soil collected just beneath each of the six infected tree species. It can be seen from Fig. 3a that the EC of the samples collected from the open field soil (OFS) were higher than those found in the nest wall soil (NWS). In addition, comparing the EC values. It can be seen from Fig. 3a that the EC values ranged from 3.6 % to 4.36 dS.m^{-1}. Furthermore, the ECs of the OFS were higher than those for the NWS significantly. Moreover, the six species studied had the same trend.

Calcium carbonate in the soil

The $CaCO_3$ compound was found naturally in the soil composition, else that belonging to the open field close to the infected trees or those collected from the nest mortar used to blend the nest wall. Because this chemical compound is well known for its binding behavior, termites use it mixed naturally with soil to enhance the nest wall' rigidity without reducing the nest wall's porosity.

The $CaCO_3$ contents of the OFS and NWS ranged from 1.008% up to 1.496% among the six species examined. In addition, it was found that the OFC's calcium carbonate content was significantly similar, as indicated in Fig. 3b.

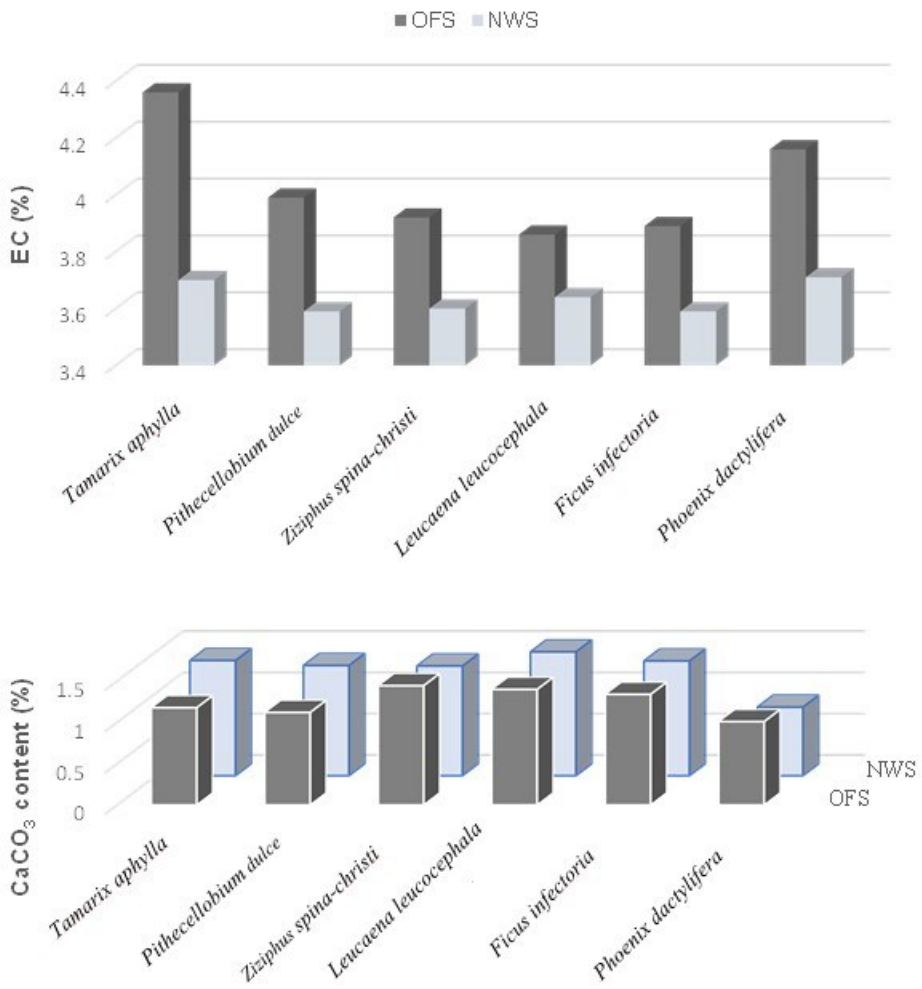

Fig. 3. Electrical conductivity (EC) and calcium carbonate content of the samples collected from open field soil (OFS) and the nest wall soil (NWS) of the six infected tree species

Soil Particles Incorporated in Nest Wall

Particle size distribution of the OFS

Table 3 and Fig. 4 show that the parent soils collected outside the termite nests just beneath each tree of the six species had the highest fractions of the coarse particles (> 425 µm) comparing to the finer particles. This trend was more obvious for both *Tamarix nilotica* and *Ziziphus spina-christi*. For the other four species sites, their major soil particles fractions were between 125 and 300 µm followed by those particles with sizes equaled higher than 425 µm.

The intact wood

The physical and chemical properties of the intact wood are presented in Table 4. Statistical analysis showed a significant difference between the six infected tree species tested concerning all the properties examined and presented at Table 4.

Regarding the SG of the intact wood, SG varied significantly due to the differences between the six tree species examined. The SG means ranged from 0.42 for *Phoenix dactylifera* to 0.71 and 0.72 for *Tamarix aphylla* and *Conocarpus erectus* wood,

respectively. Moreover, the remaining tree species occupied a median level of the SG's scale. (Table 4).

Concerning the ash content of wood, the woody polymeric tissues examined in the present investigation were significantly different in their contents of ash. Two of them contained the highest ash value (6.71% and 5.43%, for *Tamarix aphylla and Phoenix dactylifera*, respectively) compared to the other species (Table 4). The other four infected species had lower ash values ranging from 1.22% to 3.8%.

The six infected lignocellulosic resources examined varied significantly from one resource to another concerning the extractives content property. The highest extractives' value resulted for *Ziziphus sp.* as well as the date palm wood (18.89% and 18.3%, respectively), followed by the *Tamarix sp*. (15.76%). On the other hand, *Pithecellobium dulce* had the lowest extractives value among the six infected woods as clear in Table 4. Although the six tree species were found to be different in their extractives' content, termites infected their trunks in a similar manner and probabilities

The holocelluloses of wood were significantly different (Table 4). *Leucaena leucocephala* and *Pithecellobium dulce* had the highest values (70.82% and 69.41%, respectively). *Tamarix aphylla* and *Phoenix dactylifera* had the lowest holocellulose values (51.8 and 53.57, respectively). In between, *Ziziphus sp*. and *Ficus infectoria* had an intermediate situation (59.5% and 61.59%, respectively) in comparison to the HC of the healthy wood. Accordingly, it can be suggested for the fast-growing species, *Leucaena leucocephala*, that its partially infected wood can be used as cellulose derivatives and/or as lignocellulosic fibers for fiber-reinforced composite materials or papermaking applications (Hindi *et al*. 2011; Hindi 2017f).

Regarding Klason lignin content (lignin), it can be seen from Table 4 and Fig. 5 that both *Tamarix aphylla* and *Ficus infectoria* contained the highest lignin values (27.9% and 22.43%, respectively). On the other hand, *Leucaena leucocephala* had the lowest lignin content (18.86%). In between, *Pithecellobium duce* and *Ziziphus spina-christi* were similar statistically in their lignin content (20.3% and 19.71%, respectively) and occupied a median level within the species studied. The results are in agreement with those encountered in annual plants, non-wood hardwood and softwood sources that were found by other researchers (Hindi *et al*. 2011; Hindi 2017 f).

The GHC ranged from 4102 cal/g to 4814 cal/g for *Phoenix dactylifera* and *Ziziphus spina-christi*, respectively. These values of the intact woody specimens lie within the traditional scale (Hindi *et al*. 2012) as shown in Table 4 and Fig. 5.

The Termite Colony

The small Najdian Termite, *Microtermes najdensis* and its life cycle of this inset are indicated in Fig. A1, showing each of male and female winged shed (queen and king) which produce eggs. Immature forms are simply shown to be in preparation of queen, secondary queen, king, developing winged forms, winged reproductives "alatase", reproductives, soldiers, and workers) Creffield 1996; Creffield 2005; Shaikh *et al.* 2021; Liu 2018).

Forty widely distributed tree species were surveyed in Hada Al-Sham and were found to be infected by this insect. The most dominant infected plants by this pest were *Tamarix aphylla*, *Pithecellobium dulce*, *Ziziphus spina-christi*, *Leucaena leucocephala*, *Ficus infectoria*, and *Phoenix dactylifera*.

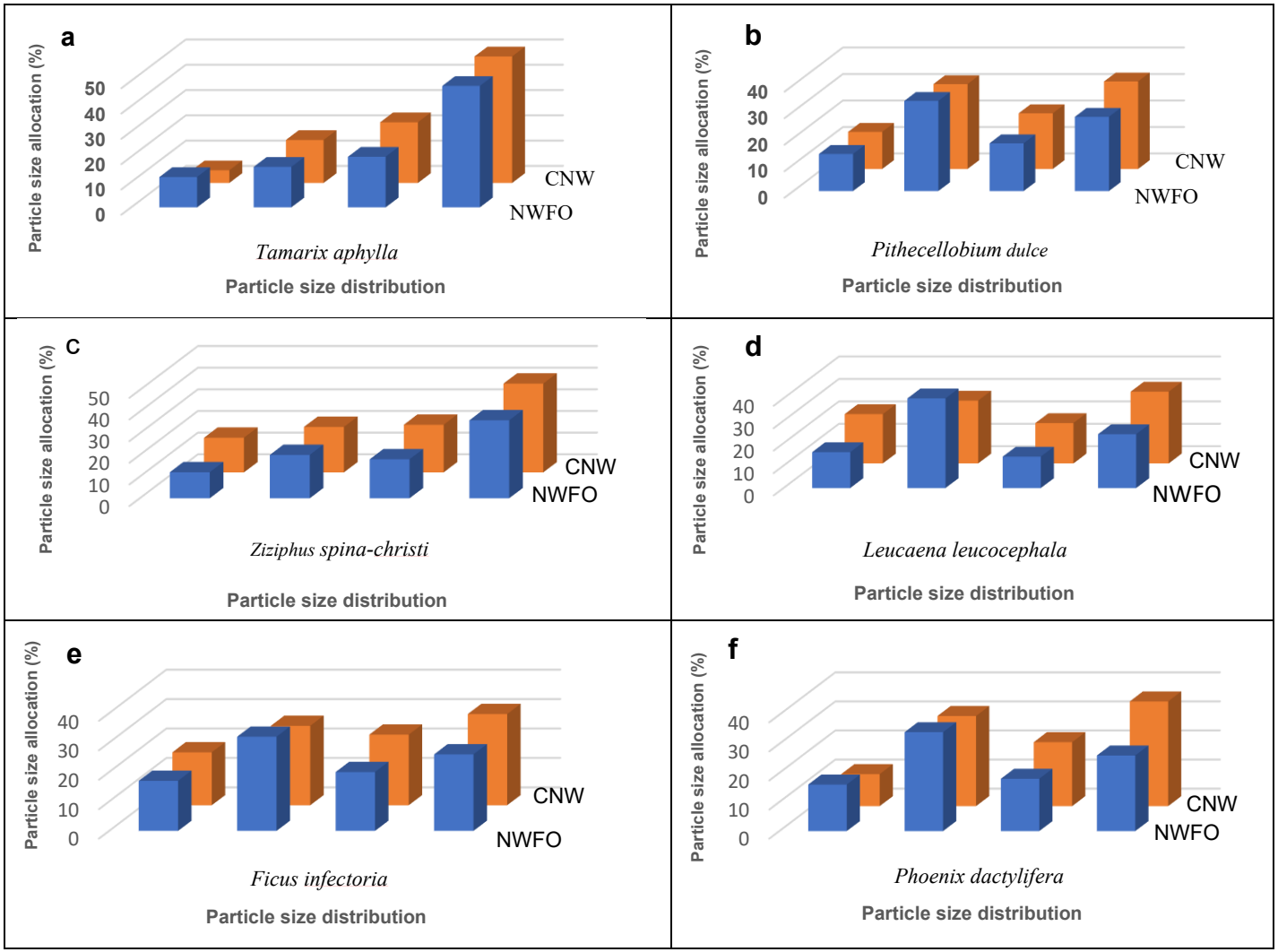

Fig. 4. Particle size allocation in the nest mortar for each of crude nest wall (CNW) and the nest wall free of organics (NWFO) for the six tree species

Table 3. Mean Values for Important Properties of the Soil Particles, Namely Size Range Allocation and Crystallinity Index for Each of Open Field's Soil (OFS), Crude Nest Wall (CNW) and the Nest Wall Free of Organics (NWFO)

Species	Soil Particle					
	Size range (µm)	Allocation (%)			[5-9] Crystallinity Index	
		OFS	CNW	NWFO	CNW	NWFO
Tamarix aphylla	< 125	12 dA	12 dA	12 dA	6.317 aB	8.903 aA
	125 - 300	16 cA	16 cA	16 cA		
	300 - 425	20 bA	20 bA	20 bA		
	425	48 aA	48 aA	48 aA		
Pithecellobium dulce	< 125	14 dA	14 dA	14 dA	5.994 aB	9.018 aA
	125 - 300	34 aA	34 aA	34 aA		
	300 - 425	18 cA	18 cA	18 cA		
	425	28 bA	28 bA	28 bA		
Ziziphus spina-christi	< 125	12 dA	12 dA	12 dA	6.108 aB	9.042 aA
	125 - 300	20 bA	20 bA	20 bA		
	300 - 425	18 cA	18 cA	18 cA		
	425	36 aA	36 aA	36 aA		
Leucaena leucocephala	< 125	16 cA	16 cA	16 cA	6.287 aB	8.989 aA
	125 - 300	40 aA	40 aA	40 aA		
	300 - 425	14 dA	14 dA	14 dA		
	425	24 bA	24 bA	24 bA		
Ficus infectoria	< 125	17 dA	17 dA	17 dA	6.009 aB	9.076 aA
	125 - 300	32 aA	32 aA	32 aA		
	300 - 425	20 cA	20 cA	20 cA		
	425	26 bA	26 bA	26 bA		
Phoenix dactylifera	< 125	16 dA	16 dA	16 dA	5.984 aB	8.994 aA
	125 - 300	34 aA	34 aA	34 aA		
	300 - 425	18 cA	18 cA	18 cA		
	425	26 bA	26 bA	26 bA		

[1] Based on oven-dry weight.
[2] Each value is an average of 3 samples.
[3] Small letters are used to compare means between species (within the same column).
[4] Capital letters are used to compare means between the CTNS and PVSS within the same species (at the same raw).
[5] Means within the same column followed by the same letter are not significantly different according to LSD at $P \leq 0.05$.

Table 4. Mean Values for Specific Gravity (SG), Ash Content (ash), Total Extractives Content (Extractives), Holocelluloses, Klason Lignin Content (Lignin) and Gross Heat of Combustion (GHC) of Wood Samples Taken from Healthy Trees of the Six Species.

Species	[1-3,7] SG (g/cm^3)	[1,2,4,7] Ash (%)	[1,2,4] Extractives %	[1,2,4] Holocelluloses (%)	[1,2,4] Lignin (%)	[1,2,5] GHC (calories/g)
Tamarix aphylla	0.71 [a]	5.43 [a]	15.76 [b]	51.8 [c]	27.9 [a]	4393 [b]
Pithecellobium dulce	0.61 [b]	3.8 [b]	6.91 [e]	69.41 [a]	20.3 [bc]	4763 [a]
Ziziphus spina-christi	0.72 [a]	1.9 [c]	18.89 [a]	59.5 [b]	19.71 [bc]	4814 [a]
Leucaena leucocephala	0.59 [b]	1.22 [c]	9.74 [d]	70.82 [a]	18.86 [c]	4206 [ce]
Ficus infectoria	0.54 [c]	2.44 [bc]	10.54 [c]	61.59 [b]	25.43 [a]	4367 [b]
Phoenix dactylifera	0.42 [d]	6.71 [a]	18.3 [a]	53.57 [c]	22.43 [b]	4102 [e]

[1] Means within the same column followed by the same letter are not significantly different according to LSD at $P \leq 0.05$.
[2] Each value is an average of 5 samples.
[3] Based on oven-dry weight and green volume.
[4] As percentage of oven-dry wood weight.
[5] Based on oven-dry weight.

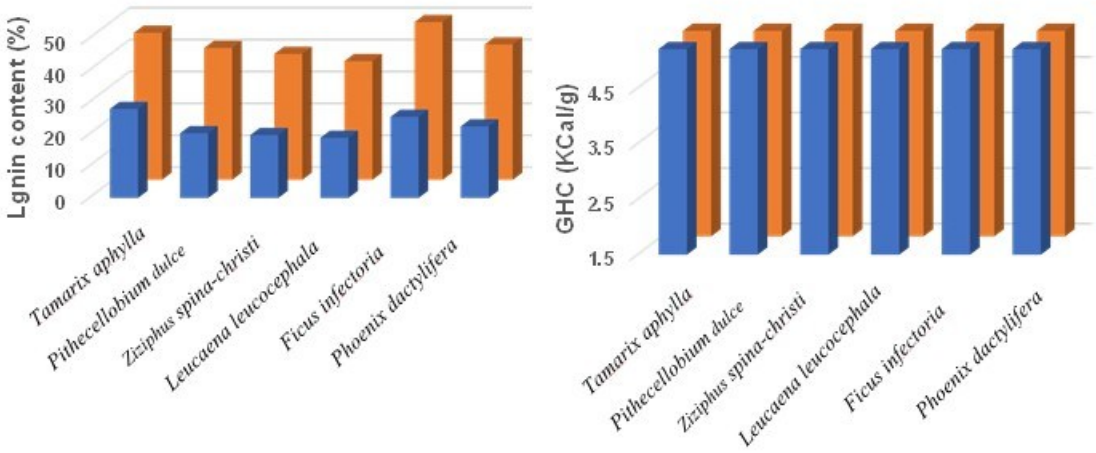

Fig. 5. Klason lignin (Lignin) content and gross heat of combustion (GHC) of intact wood (blue histograms) and the nest wall (orange histograms) of the six infected tree species.

The infection aspects of *Ziziphus spina-christi*'s wood infected by the Najdian Termite, *Microtermes najdensis* are shown in Fig. A1.

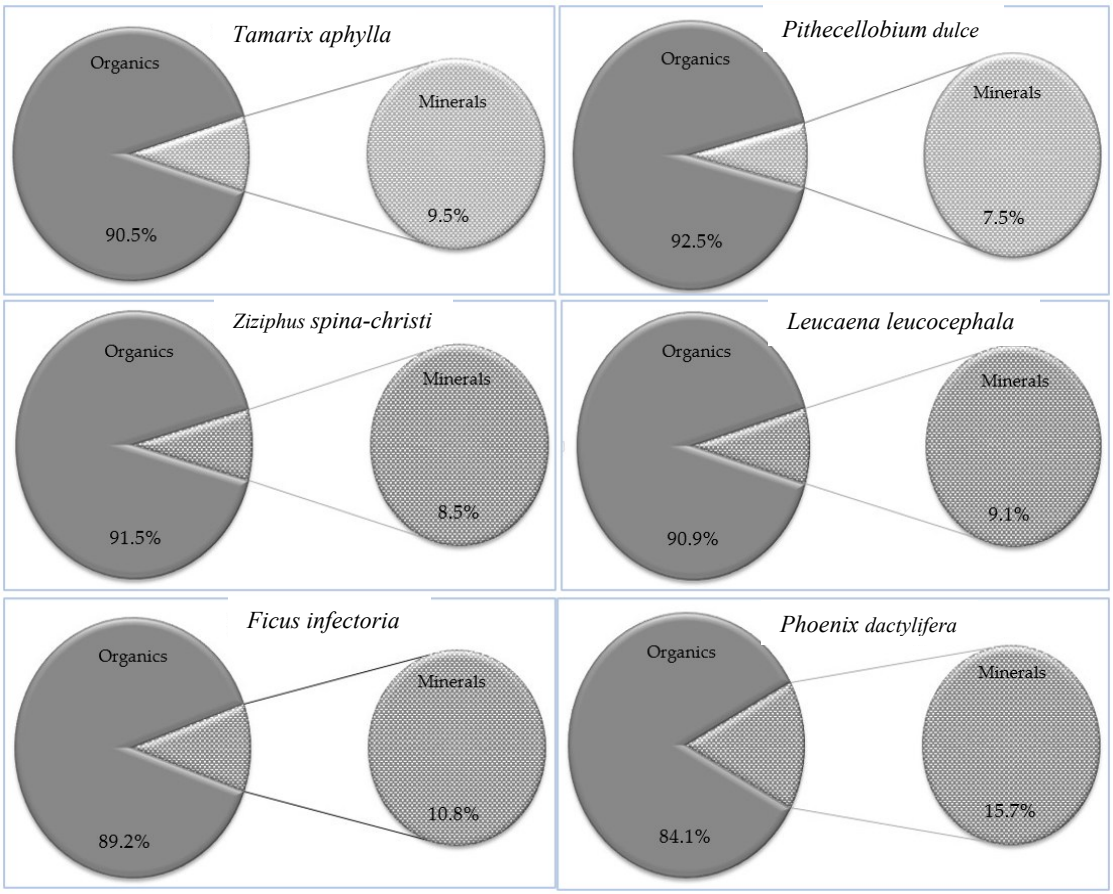

Fig. 6. Organic matter content (organics) and mineral content (minerals) of the nest wall occupied trunks of the six tree species

Organic Matter and Mineral of the Nest Wall

The mineral content that was determined according to the related standard methods of the nest mortar ranged from 84.1% for *Phoenix dactylifera* to 92.3% for *Pithecellobium dulce* (Fig. 6). In addition, the minerals are considered as the most abundant constituent of the termite nest mortar. These results agree with those indicated by Ptáček *et al.* (2013) and Rückamp *et al*. (2011).

The organics of the nest mortar ranged from 7.7% for *Pithecellobium dulce* to 15.9% for *Phoenix dactylifera* (Fig. 6). There is no correlation between the organics and the lignin content of wood.

Lignin Content in the Nest Wall

Figure 7 shows the allocation of both organics and lignin from old nests (lignin-O) and recent nests (lignin-R) skeletons within the trunks of the six infected tree species.

Both organics and lignin contents were higher in termite nests than those of the reference soil (Fig. 7).

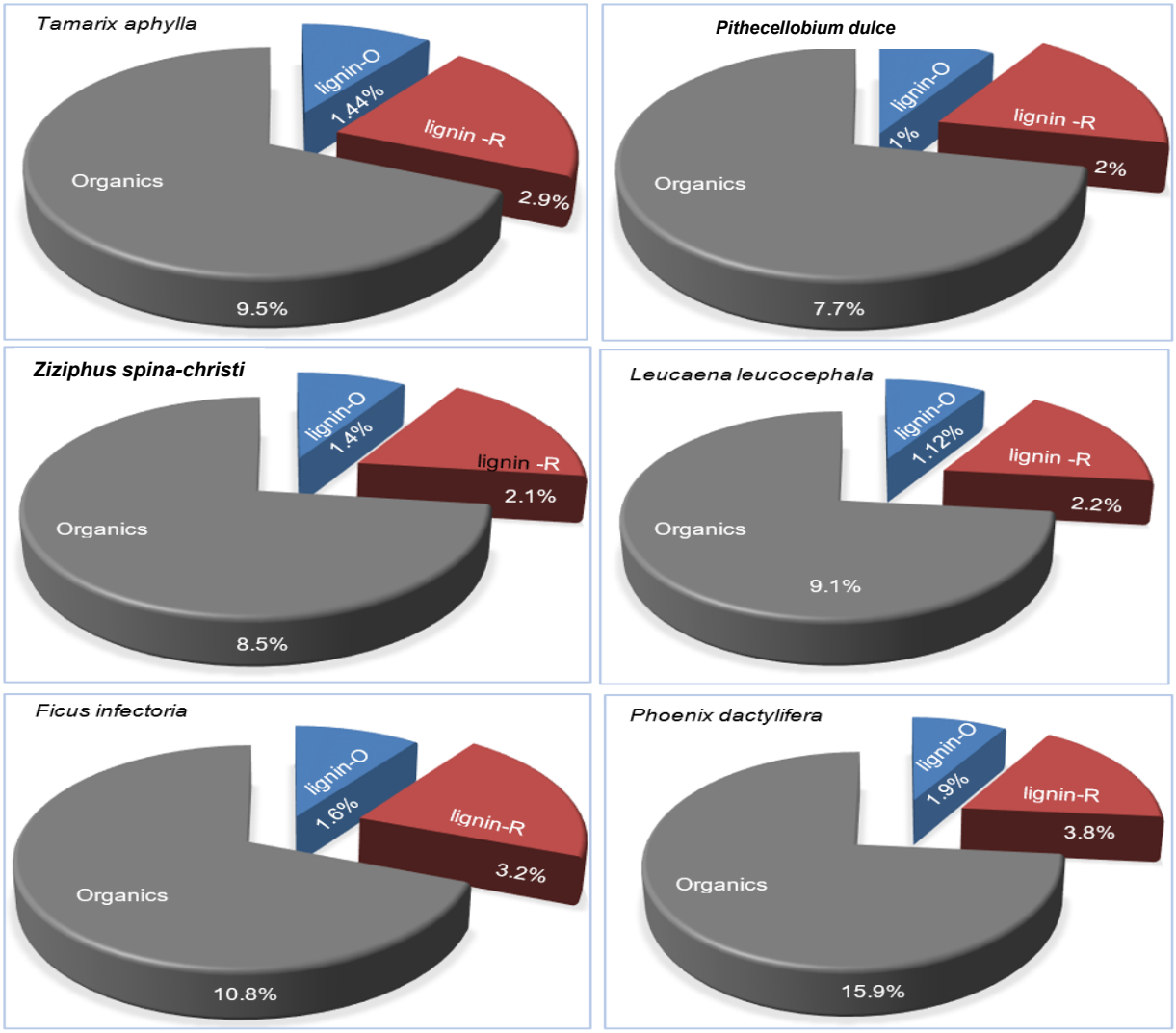

Fig. 7. The allocation of organic matter content (organics) and the Klason lignin (lignin) content from older nests (lignin-O) and more recent nests (lignin-R) skeletons within trunks of the six infected tree species

Nanocelluloses Reinforcing the Nest Wall

The nest wall's samples were examined spectroscopically by SEM technique in order to speculate their surface morphology and types of anatomical features as presented at Fig. 8 (for the MCC's microparticles) and Fig. 9 for the NCC's nanoparticles (Hindi 2017c,d).

The MCC

Depending on Hindi (2017 c,d), excess investigation of the six nest wall specimens collected from the six tree species was achieved. In addition, SEM, FTIR, and XRD examinations were performed to confirm the presence of the MCC and NCC in the nest's mortar as a secondary binder agent.

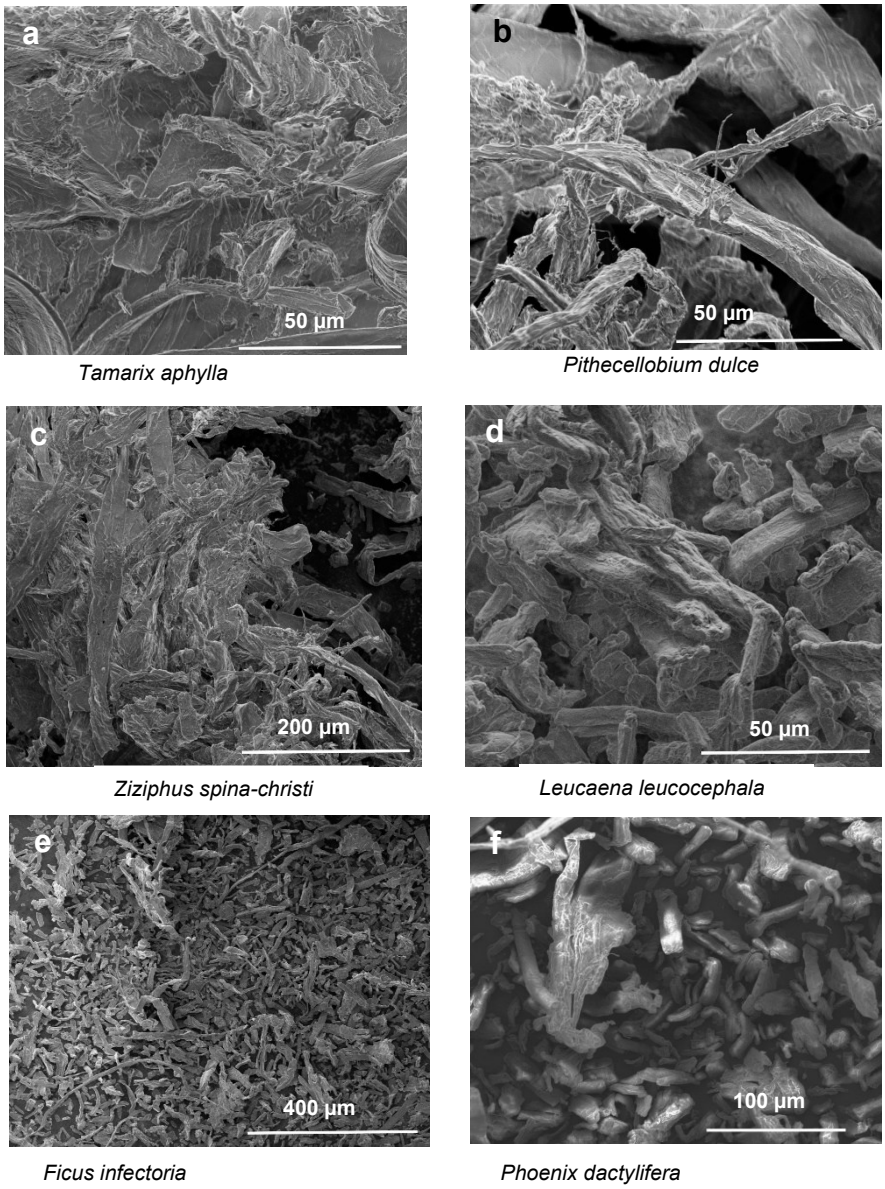

Fig. 8. SEM micrographs of the microcrystalline cellulose (MCC) synthesized naturally by termites' enzymatic hydrolysis of cellulose as detected in the nest wall within the six infected tree species

Concerning to the SEM micrographs shown in Fig. 8, all the six subfigures (a-f) are presented in a micrometric scale ranged gradually from 50 µm (*Tamarix aphylla*, *Pithecellobium dulce*, and *Leucaena leucocephala*), 100 µm (*Phoenix dactylifera*), 200 µm (*Ziziphus spina-christi*), and 400 µm for *Ficus infectoria*. This difference in magnification between the subfigures resulted from an attempt to reach the best resolution. Moreover, it is noted that the SEM' dimensions for both MCC and NCC were less accurate to depend on comparing to the other tools (FTIR and XRD).

The NCC

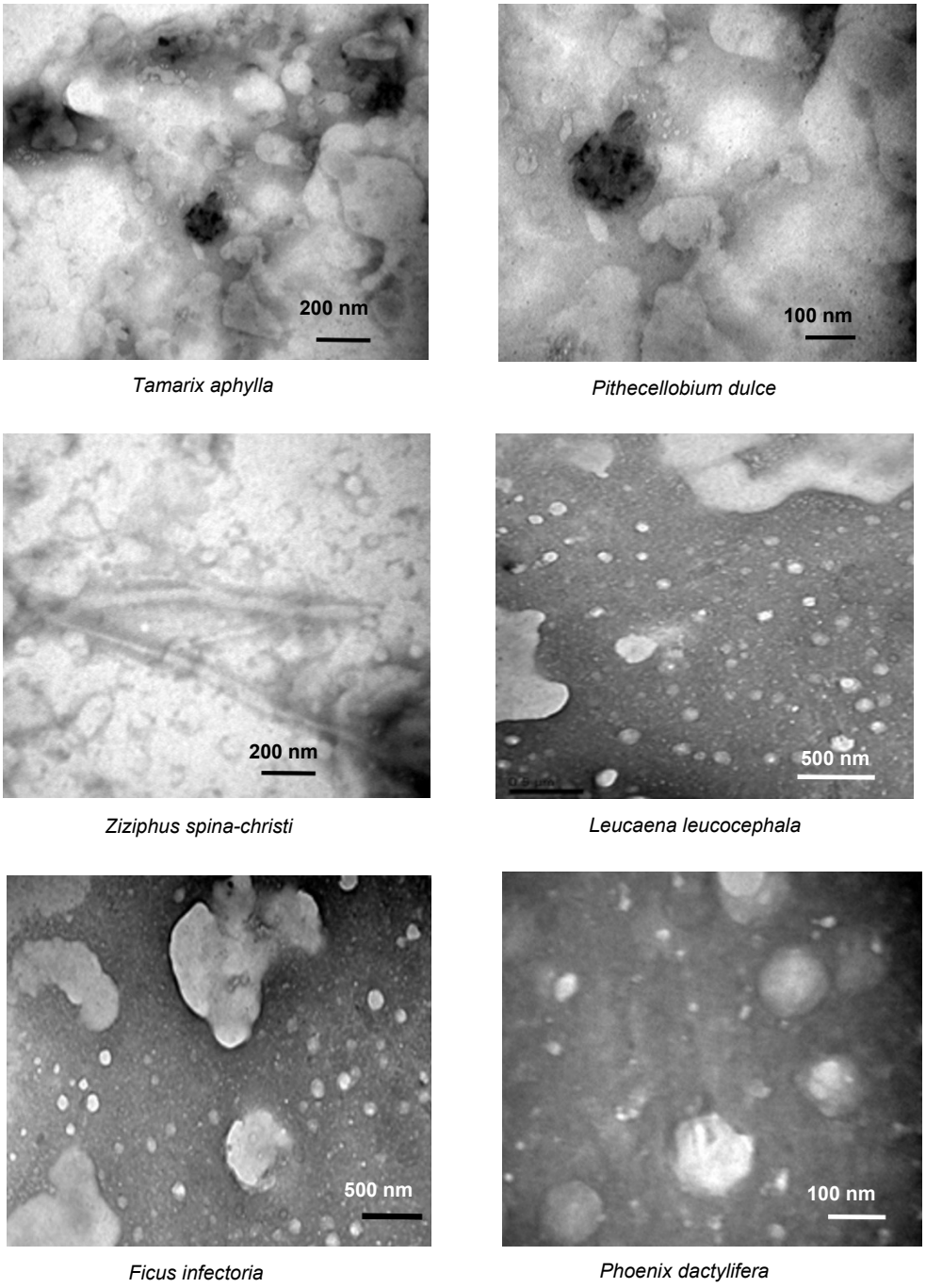

Fig. 9. TEM micrographs of the nanocrystalline cellulose (NCC) synthesized naturally by termites' enzymatic hydrolysis of cellulose as detected in the nest wall within the six infected tree species

FTIR

The FTIR's spectrum of each alpha cellulose (C_α) and its nanocelluloses products, namely MCC and NCC for the six tree species examined are presented in Fig. 10.

Table 5. Common Absorption bands and Their Reasons for the Alpha Cellulose (C_α), MCC, NCC within the Six Infected Tree Species

Wavenumber (cm^{-1})	Reason for Band Appearance
1050	C–C ring stretching band and C–O–C glycosidic ether band.
1283	Scissoring motion of the CH_2-group.
1583	O-H bending of the absorbed water.
1658	C-O stretching vibration for the acetyl and ester linkages.
2850	C-H stretching.
3367	O-H stretching (axial vibration) intramolecular hydrogen bonds.

The above-mentioned explanation of the originality of both MCC and NCC from cellulose can be extended through studying their FTIR-bands (Fig. 10) and reasons of their arisen at certain wavenumbers (Table 5) as indicated by Hindi (2017 b,c,d).

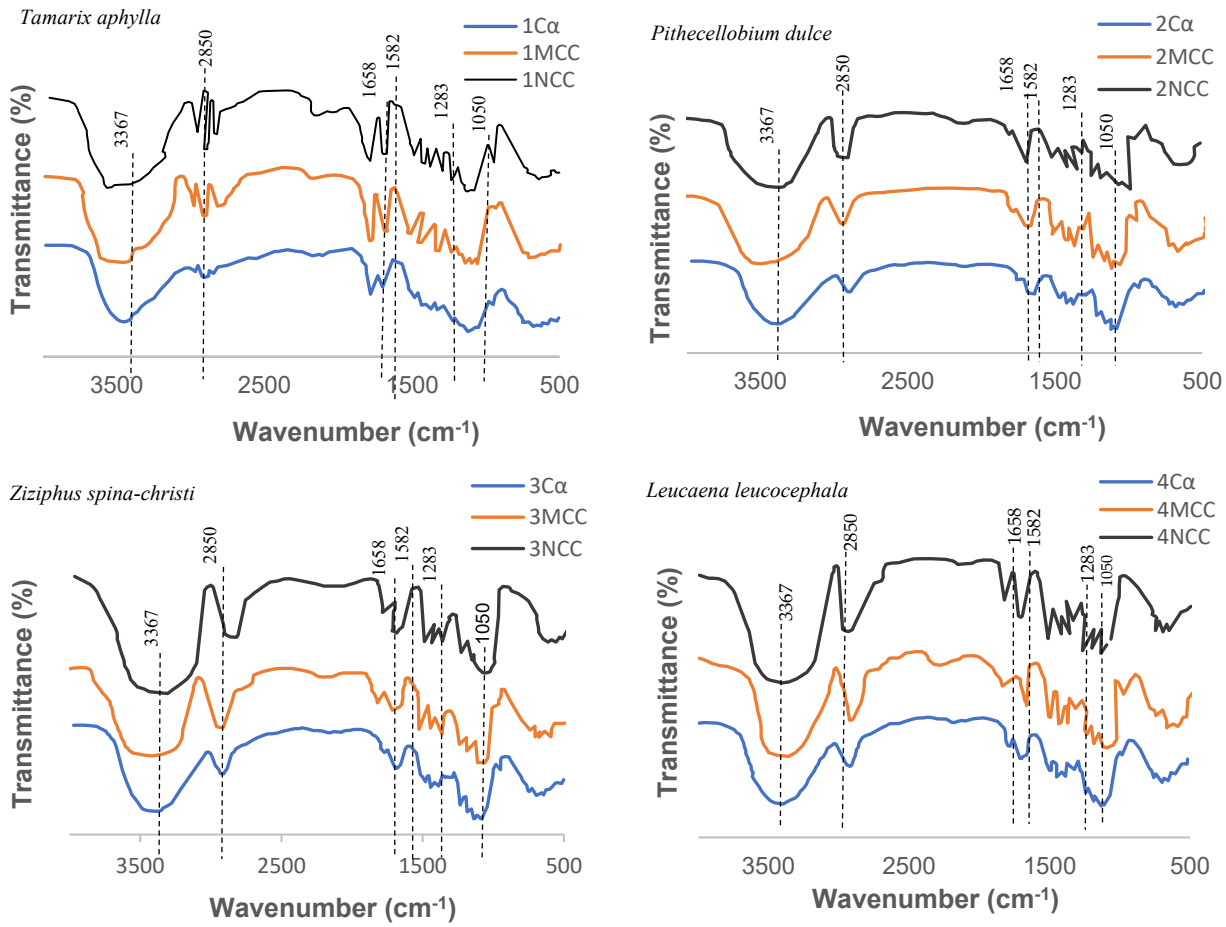

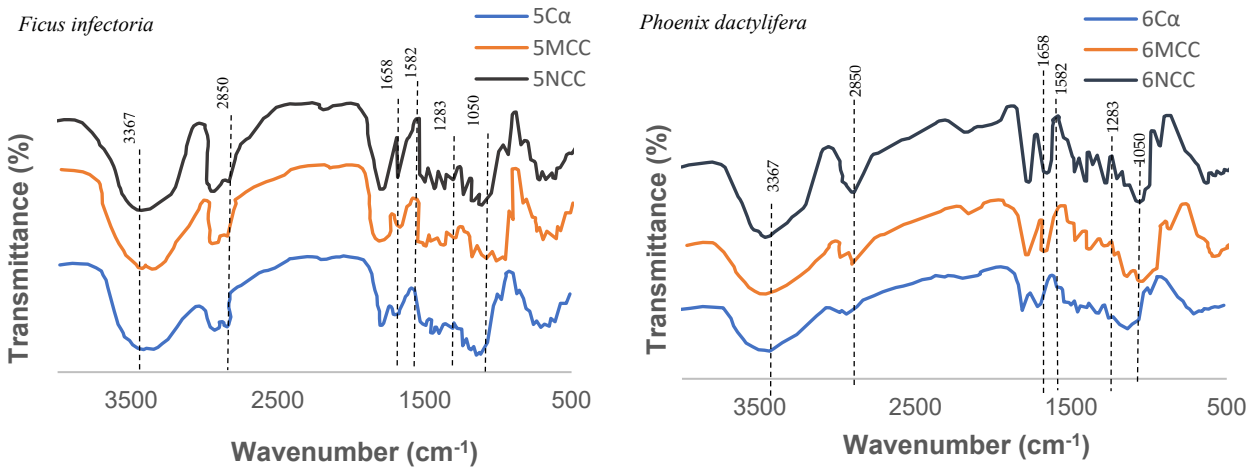

Fig. 10. FTIR spectra of the alpha cellulose (C_α), MCC, NCC within the six infected tree species

XRD

As shown in Fig. 11, the crystallinity index was increased from crude wood passing through alpha cellulose, MCC and, finally ended by the NCC.

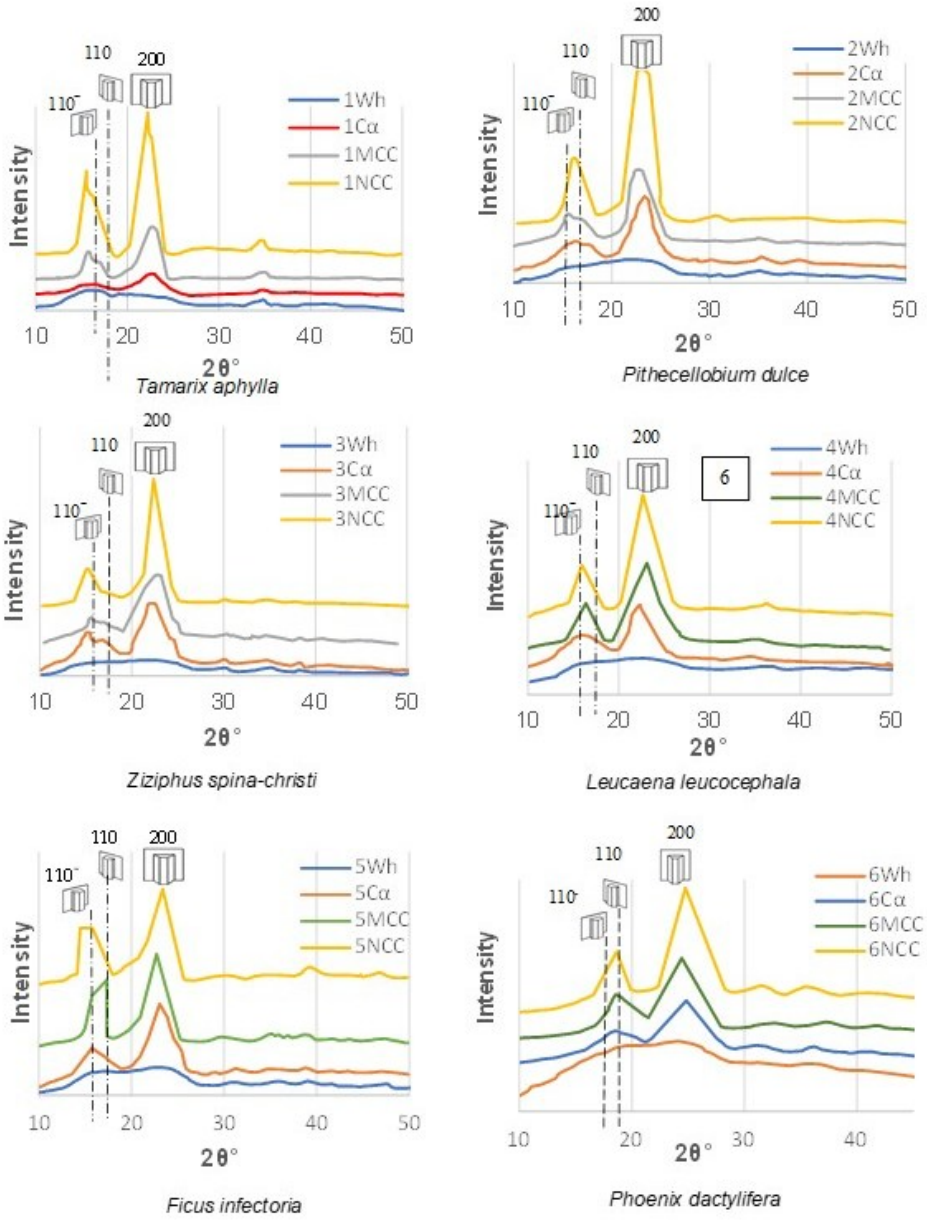

Fig. 11. X-ray Diffractogram (XRD) of the healthy wood (W_h), alpha cellulose (C_α), microcrystalline cellulose (MCC), nanocrystalline cellulose (NCC) within the six infected tree species

Mechanical Properties of the Nest Wall as Affected by the Polymeric Blend

The mechanical properties of the modulus of elasticity (MoE), namely compressive stress and MoE of the six infected tree species are presented in Fig. 12.

Stress–strain relationship of the nest wall

The histograms presented at Table 6 and Fig. 12 revealed that the ultimate compressive stresses (UCS) of the nest wall constructed in the six infected tree species were differed significantly among species (Liu 2018; Zachariah *et al.* 2020).

The mean values of proportionality limit (PL) and ultimate compressive stress (UCS) are presented in Table 6 and Fig. 12. The PL values were found to be ranged between 0.814 to 1.12 MPa for *Pithecellobium dulce* and *Leucaena leucocephala*, respectively. Moreover, the UCS the six infected tree species differed from 1.73 MPa up to 2.09 MPa for *Phoenix dactylifera* and *Leucaena leucocephala*, respectively.

Table 6. Proportionality Limit (PL) and Ultimate Compressive Stress (UCS) of the Six Infected Tree Species

Species	Stress Type	Stress (MPa)	Strain
Tamarix aphylla	PL	0.865 ± 0.064	0.188 ± 0.054
	UCS	1.973 ± 0.183	0.58 ± 0.024
Pithecellobium dulce	PL	0.814 ± 0.059	0.375 ± 0.023
	UCS	1.992 ± 0.117	0.878 ± 0.041
Ziziphus spina-christi	PL	0.84 ± 0.066	0.301 ± 0.027
	UCS	2.037 ± 0.083	0.805 ± 0.045
Leucaena leucocephala	PL	1.116 ± 0.071	0.305 ± 0.019
	UCS	2.092 ± 0.088	0.858 ± 0.046
Ficus infectoria	PL	0.936 ± 0.062	0.339 ± 0.037
	UCS	1.987 ± 0.048	0.685 ± 0.033
Phoenix dactylifera	PL	0.664 ± 0.039	0.251 ± 0.016
	UCS	1.733 ± 0.064	0.927 ± 0.034
Each value is an average of 3 samples ± standard deviation.			

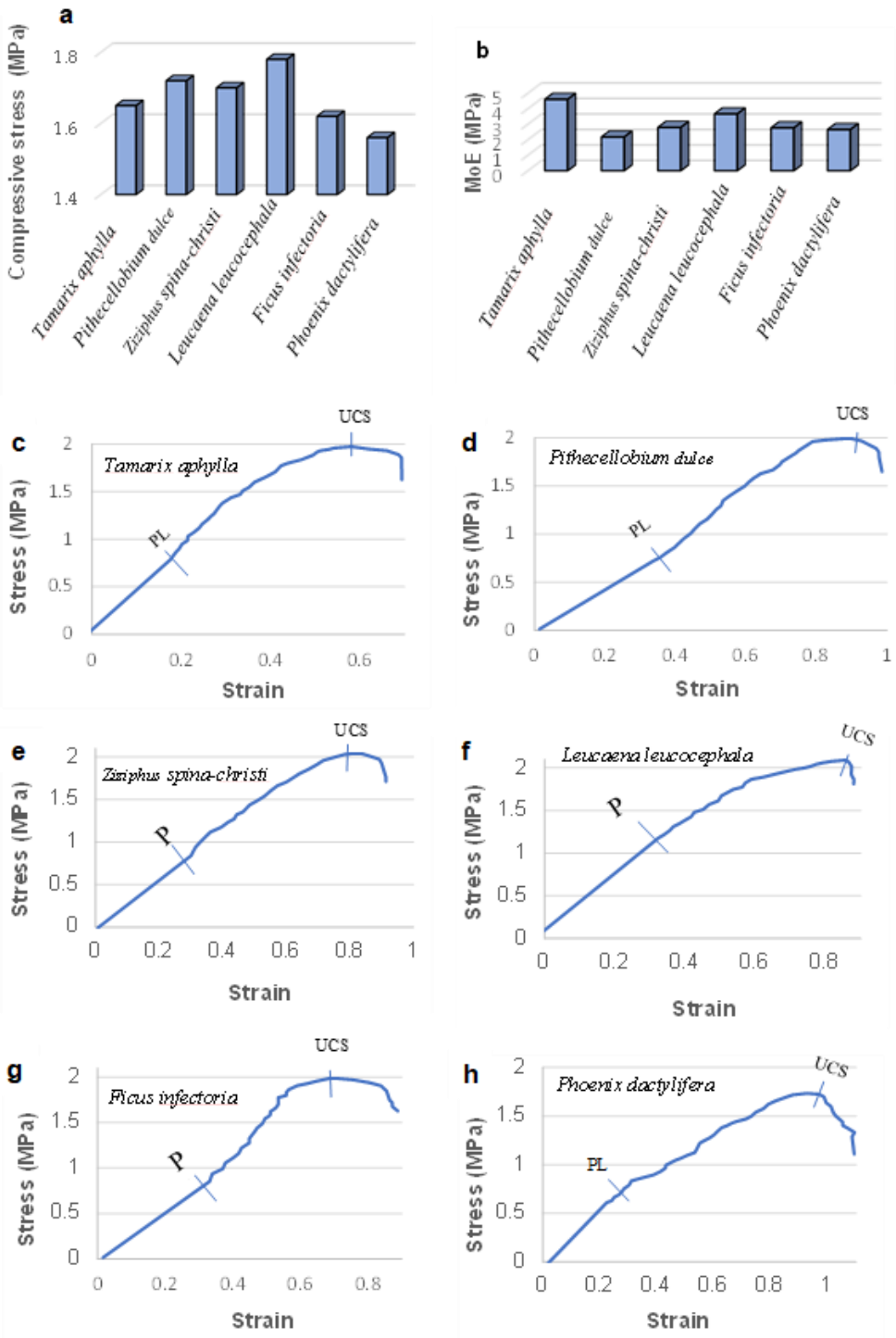

Fig. 12. Mechanical properties of the nest wall skeleton: a) Ultimate compressive stress (UCS) and b) Modulus of Elasticity (MoE) and c–h) Stress–strain graphs of the nest wall constructed in: **(c)** *Tamarix aphylla*, **(d)** *Pithecellobium dulce*, **(e)** *Ziziphus spina-christi*, **(f)** *Leucaena leucocephala*, **(g)** *Ficus infectoria*, and **(h)** *Phoenix dactylifera* showing proportionality limit (PL) and ultimate compressive stress (UCS).

DISCUSSION

Studying the Termite System

Atmosphere

As shown in Table 1 and Fig. 1, January was the coldest month throughout the investigation period (October 2019 to August 2021) that stresses termites due to low temperatures. The meteorological data of this month are presented in Table 1.

Concerning the relationship between the internal temperature (IT) and outer temperature (OT), it was identical for all the eleven graphs representing the 11th months of the measuring period. This common trend indicates that termites prefer warmer atmospheres other than the colder one that is expected that coldest nest may affects termite members' activity, especially their young (Fig. 2).

Soil

Concerning the soil, the significant similarities between the OFS and NWS reflects that their soil were in correspondence and origin.

According to Fig. 3b it was demonstrated that termites took soil particles mixed with calcium carbonate and blended it with nest's mortar. Both termites and soil calcium carbonate play important roles in the global carbon cycle: termites produce methane and break down organic matter, while soil calcium carbonate stores carbon dioxide from the atmosphere. These two elements may combine in arid and semiarid soils through termites' biomineralization of calcium carbonate (Liu *et al.* 2007). It was found by Liu *et al*. (2007) that termite galleries do not always include carbonate. It only happens in galleries where there is subsurface carbonate within 100 cm of the surface. Termite galleries usually had carbonate ratios of $^{13}C/^{12}C$ that matched subsurface carbonate ratios. Calcite is the carbonate mineralogy found in all galleries, soils, and termites themselves, according to X-ray diffraction. In addition, carbonate was found in the termite gut together with other soil particles and plant opal, according to thin sections, scanning electron microscopy, and X-ray mapping. Every test supported the upward-transport theory and refuted the biomineralization idea. Since the gallery carbonate was formed by upward movement, we deduce that it contributes less actively to short-term carbon sequestration than it would have if the termites had biomineralized it directly.

In addition**,** concerning the soil particles incorporated in the nest wall, it was thought that using coarser soil particles in the mortar blended with fine particles of organic materials, lignin and nanocellulose (MCC, NCC) made it possible to fabricate more permeable nest wall featured by its high gas exchanging (Table 3 and Fig. 4).

Examining Table 3 and Fig. 4, it can be indicated that termite workers use this coarse particle size (> 425µm) more than the finer ones that allow better ventilation within the nest.

An intuitive question that might arise in the minds of ordinary readers are "what particles' size can this insect remove?" Other related questions are "how can these insects grade the sandy particles?" as well as "how can they transfer the fine particles", and finally, "where do they get rid of the fine sandy garbage?,"

Since we ensure that these insects don't have electromechanical sieves to separate the different particle sizes, we guess that their mortar-composite blended with their saliva, lignin, MCC and NCC are responsible for agglomerating a portion of fine particles to become coarser. Based on this guess, the coarse soil's particles were supposed to be divided into two categories: the parent virgin soil particles and the composite based-coarse particle. However, further studies are required to confirm this expectation using XRD analysis.

Accordingly, the coarse soil's particles were guessed to be divided into two categories: the parent virgin soil particles and the composite based-coarse ones. However, further examination was added to confirm this expectation using XRD analysis. In addition, it was explained how the porous structure of the nest's walls can be fabricated by the so-called "Baking phenomenon" initiated from while releasing the fluidic components of the mortar composite blended by termites (water steam and gases) just upon curing and before hardening of such polymeric blend. Finally, the authors regard this is a very important finding that can help in the study of biomimicry.

The tree species

Lower SG values indicate that their cell wall backbone is expected to be penetrated by termites more easily digesting their carbohydrate contents compared to the other lignocellulosic tissues with higher SGs (Table 4).

According to the continuous monitoring of study area at Hada Al-Sham region, termites infected the six hardwood species irrespective of their contents of ash, as is clear from Table 4. Concerning the partially infected wood, it must be directed to any economic applications. It is worth mentioning that the chemical recovery application will be significantly impacted by high ash concentrations, which could be a significant disadvantage (Hindi *et al*. 2011). The findings, however, agreed with those found in other publications.

Examining Table 4, when searching about the possibility of using the partially infected wood in a certain industrial application such as fiber production and/or domestic utilization such as firewoods, the presence of high extractives into the lignocellulosic tissues is unpreferred in the industrial sector due to their interference with the chemical reagents used in that application (Hindi *et al*. 2011). Accordingly, the extractives of wood must be organic solvent-extracted before manufacture, thus step will add additional cost to this industry.

Based on the results presented at Table 4 and Fig. 5, the partially infected timber trees are more suitable for reusing in fiber production as well as renewable energy resources comparing to the date palm species although the later the most abundant raw material in Saudi Arabia. The best resource is *Leucaena leucocephala* because of its high holocellulose content, appropriate fiber length, and specific gravity that is similar to that of hardwoods. In comparison to the other resources we looked at, it has less lignin, ash, and total extractives. In addition, compared to other woody raw materials, lignocellulosic materials with low lignin content have shorter pulping times and lower chemical charges (Diaz *et al*. 2007; Lopez *et al*. 2008). Additionally, it is anticipated that the pulp industry will use more chemicals at greater lignin contents (Khristova *et al*. 2005; Hindi *et al*. 2011).

Based on GHC output, it can be suggested that partially infected wood can be directed to the energy sector to generate heat for domestic and industrial applications. In addition, this utilization helps to discard any traces of these dangerous insects (Table 4 and Fig. 5).

The nest wall

It can be seen from Fig. A1 that termite started to infect the sapwood, other than the heartwood of the infected log. This aspect is attributed to the fact that heartwood is more resistant to the termites' infestation due to its high content of the organic extractives compared to the sapwood. In addition, the bark of the infected *Ziziphus* tree was swollen and peeled easily due to the prominence of the tunnels shielded by a ceiling made up of a

thick layer of the mortar. In addition, huge number of entryways are noticed in the southwest direction. This direction was not selected by termites fortuitously, but they allowed their nests to have better aeration and more efficient gas exchange achievement.

Regarding the chemical structure of the nest wall, it was reviewed that termites feeding on wood use easily degradable cellulose components rather than lignin as carbon and energy source. Since lignin resists degradation by most termite species, it could be a prominent tracer of the organic matter incorporated into termite nests and released into nest surroundings (Ptáček *et al*. 2013 and Rückamp *et al*. 2011). Recent nests have more lignin contents compared to the older ones since it is degraded with increasing of the nests' age (Fig. 7). Moreover, the lignin was even more enriched than that found in the termite nest mortar. This is due to termite's use of lignin as the main organic binding agent in the nest mortar (Fig. 7).

The nanometric-cellulosic materials (resembling MCC and NCC) were surprisingly found to be synthesized naturally by the act of hydrolyzing enzymes of the fungal communities and/or the termites' digestion detected within the nest wall within each of the six infected tree species (Fig. 8 and 9). It was shown by using SEM and TEM imaging that the form and crystalline content of cellulose within the termite dwelling appeared similar to the known MCCs and NCCs derived by acid hydrolysis of delignified wood.

It is worth mentioning that optical microscopy makes it possible to select a certain magnifying lens and standardize imaging as well as anatomical measurements that is useful for comparison purposes. On the other hand, concerning standardization for SEM and TEM, it is practically difficult or may be impossible due to one or more of the following reasons: 1) electron beam settings: The operating conditions such as beam voltage, spot size, and working distance can affect the apparent magnification, b) sample topography: Variations in sample surface texture and height can influence effective magnification, and 3) detector configuration. The type of detector (*e.g*., secondary electron detector, backscattered electron detector) can also impact on the perceived image size. It is worth mentioning that the main object of imaging both MCC and NCC in the present study is to detect and confirm the presence of them as nanometric byproducts of the enzymatic hydrolysis occurred naturally by micro-organisms live within termites' stomach.

The data obtained from the MCC and NCC materials were presented at Figs. 8 to 11 for SEM, FTIR, and XRD, respectively. All the above-mentioned analyses tools confirmed that the micro- and nano-metric particles detected were MCCs and NCCs.

This difference in accuracy for the SEM's image dimensions is attributed to the crystal growth phenomenon discovered previously by Hindi (2017 c,d) for NCC. Figure 9 shows that the scale bar of the six SEM's images for the NCCs ranged from 100 to 500 nm (Hindi 2017a-d, 2018, 2020, 2021, and 2022a,b; Shaikh *et al.* 2021). These dimensions are greater than those legally accepted according to Hindi (2017c), who reported that nanocellulose must have at least one dimension less than 100 nanometers in size. The NCC's dimension always starts from about 5 nm, and after that the nanoparticle's dimension increases through a self-process termed as crystal growth (Hindi 2017c,d). This crystal development process from nano- to micrometric size demonstrated the NCCs' aptitude for self-organization, or so-called self-assembly. After about 30 min of spreading a drop of the hydrolysis supernatant onto the sample holder (stup) of the SEM microscope, the NCCs spherulites were agglomerated into larger aggregates of colloidal state, which were then aligned straight to form a needle-shaped architecture.

The driving force for this crystal growth process can be limited to the following effects: a) electrostatic forces on the NCCs surfaces due to the grafted functional groups

(protons, sulfate, and hydroxyl), b) the concentration gradient of the fungal communities' hydrolyzing enzymes and/or termite digestion, and c) the difference in surface tensions of solution, air, and glass. The net force produced at this interaction is thought to be the driving force behind the NCCs-crystal formation process. As a result, the needles were conceived to be created through electrostatic end-to-end attraction and subsequent self-welding of small NCC particles into larger ones (Hindi 2017a-d, 2020; Hindi and Abohassan 2018). However, it can be noticed from Fig. 9 that there was a wide variation in particle size of the NCCs, which confirms the present theory of the NCC's crystal growth.

Because nanocelluloses incorporated within the nest wall' mortar was discovered for the first time, it was expected that this phenomenon is one of the important reasons that strengthen the nest wall that helps them to endure different environmental stresses.

Moreover, the scientific illustration of their FTIR spectra was concluded at Table 6 showing the absorption bands of chemical (functional) groups featuring the examined cellulosic materials. All the samples exhibited two main absorbance regions detected (800 to 1800 cm^{-1} and 2800 to 3500 cm^{-1}). The FTIR spectra of all samples has shown sharp bands around the wavenumbers (Hindi 2017 c,d) as presented in Table 5.

Based on the FTIR'S spectral data for C, MCC, and NCC materials arisen from each of the six tree species (Fig. 10), the principal constituent of the three cellulosic materials (C_{α}, MCC, NCC) were like each other's, which means that the nanometric particles detected (MCC and NCC) were nanocelluloses (Table 10).

This finding also confirms the presence of the nanocellulose in the six mortar blends as a result of enzymatic hydrolysis occurring by termites and/or fungi during their feeding and constructing their nests (Fig. 11).

These differences in PL and UCS of the nest wall' of the infected specimens collected from the six species may be attributed to their differences in densities and the chemical properties of the parent materials constituting the nest wall' backbone (Table 6 and Fig. 12).

Scientific Theory of "Wall Fabrication of Termites' Nest"

Based on the above-mentioned outcomes of this study, a scientific theory covering building termite's nest engraved in/beside lignocellulosic resource as follows:

1. After the termite community reaches a suitable site that often suffers from dryness, they collaborate with accompanying fungi. The termite community selects the most susceptible trees for infection which are, often, trees suffering from drought stress.
2. They begin engraving their nest having various entrances, first with sapwood (an outer-zone wood) and moving into heartwood (an inner-zone wood).
3. During the building process, they transfer soil particles from the nearby sites to the infected tree.
4. Upon their feeding on the woody tissues by themselves and-or by their assistant fungi, remainder wastes (lignin and cellulosic matter resembling MCC and NCC) produced from enzymatic hydrolysis of the cellulose are used by termite for constructing their nest walls. Lignin is used as the essential natural binder for soil particles beside calcium carbonate binder. In addition, the MCCs and NCCs are used to reinforce the mortar of the nest wall that promotes more strength to the nest wall.

5. While curing the nest wall's mortar, it appears that CO_2-gas is emitted because of fermentation of some biological waste presented inside the nest. This gas is thought to be responsible for the permeability of the nest wall. This is called a baking process. While curing the nest wall's blend and before its hardening, termites engrave the entryways of the nests in the southwest direction that promotes better ventilation.

CONCLUSIONS And FUTURE PROSPECTIVES

The composition and quality of the tunnels' mortar made by the Najdian Termite, *Microtermes najdensis* were extensively studied in the present investigation. Climate, soil, healthy wood (Wh) as well as the nest wall engraved within the prevalent infected timber trees were the four components of the termite system that were investigated physically, chemically and spectroscopically.

1. The entryways of the termite nests were noticed to be located at the southwest direction for all the infected that promotes better ventilation.
2. The internal temperature of the nests was recorded to be milder than the outer temperature on hot days and *vice versa*. This finding reflects that termites prefer hotter atmospheres than colder circumstances.
3. Lignin was shown to be the prominent binder for the mortar.
4. A natural enzymatic hydrolysis was suggested to be occurring within the termites' stomach by the aim of fungi that responsible on secreting the degrading enzymes producing microcrystalline cellulose and nanocrystalline cellulose as discovered for the first time in the termite nest mortar that promotes more strength to the nest wall.
5. The reasonable calorific value of the infected wood opens the door for practical utilization of such materials to be used as renewable energy resources instead of disposal them without economic benefits.
6. These findings can help in the interpretation of termite nests' durability to different environmental stresses.
7. Biomimicry of the termites' nest construction can lead to modifying the current construction's designs to be greener and ecofriendly.
8. For future prospectives, it is recommended to study termite feces. It would be interesting to find out whether they share lignin and organic compounds' composite used to blend the nest skeleton or spit it out. This will be useful to enrich the scientific information needed to accurate biomimicry of the eco-friendly ideal our buildings.

ACKNOWLEDGMENTS

The authors are grateful for the support of the Deanship of Scientific Research (DSR), KAU, Jeddah under grant no. G 155-002-1433.

REFERENCES CITED

Al-Ghamdi, K. M., Aseri, A. A., and Mayhoub, J. A. (2009). "Field study on tunnel shapes of the small Najdian Termite, *Microtermes najdensis* (Isoptera: Macrotermetidae) and the percentage of infestation in its host plants in Makkah Al., Mokaramah Province," *JKAU; Met. Env. Arid Land Agric. Sci*. 20 (1), 23-43.

Arshad, M. A. (1981). "Physical and chemical properties of termite mounds of two species of Microcerotermes (Isoptera: Termitidae) and the surrounding soils of the semi-arid Savanna of Kenya," *Soil Sci.* 132, 161-174. DOI: 10.1097/00010694-198108000-00006.

Asiry, K. A., Nurul Huda, Md., and Mousa, M. (2022). "Abundance and population dynamics of the key insect pests and agronomic traits of tomato (*Solanum lycopersicon* L.) varieties under different planting densities as a sustainable pest control method," *Horticulturae* 8, article 976. DOI: 10.3390/horticulturae8100976.

ASTM D 1105-84 (1989). "Standard method for preparation of extractive-free wood," ASTM International, West Conshohocken, PA, USA.

ASTM D 1106-84 (1989). "Standard test method for acid-insoluble lignin in wood," ASTM International, West Conshohocken, PA, USA.

ASTM. D 2015-85 (1987). "Standard test method for gross calorific value of coal and coke by the adiabatic bomb calorimeter," ASTM International, West Conshohocken, PA, USA.

ASTM. D 2395-84 (1989). "Standard test method for ash in wood," ASTM International, West Conshohocken, PA, USA.

ASTM D 2974 - (1989). "Standard test methods for moisture, ash, and organic matter of peat and organic soils," ASTM International, West Conshohocken, PA, USA.

Badawi, A. I., Faragalla, A. A., and Dabbour, A. I. (1982). "The role of termites in changing certain chemical characteristics of the soil," *Sociobiol*. 7, 135-144. DOI: 10.1071/SR9900055

Badawi, A., Al-Kady, H., and Faragalla, A. A. (1986). "Some factors affecting the distribution and abundance of termites in Saudi Arabia," *Anz. Schadlingskde., Pflanzenschutz, Umweltschutz.* 59, 17-19. DOI: 10.1007/BF01903143.

Balkhair, K. S., and Ashraf, M. A. (2016). "Field accumulation risks of heavy metals in soil and vegetable crop irrigated with sewage water in western region of Saudi Arabia," *Saudi J. of Biol. Sci*. 23, S32-S44". DOI: 10.1016/j.sjbs.2015.09.023

Chouvenc, T., and Su, N.-Y. (2012). "When subterranean termite challenge the rules for fungal epizootic," *PLoSOne* 7, article e34484. DOI: 10.1371/journal.pone.0034484

Collins, N. M. (1981). "Consumption of wood by artificially isolated colonies of fungus-growing termite *Mastotermes bellicosus*," *Entomol. Exp. Appl*. 29, 313-320. DOI: 10.1111/j.1570-7458.1981.tb03074.x.

Creffield, J. W. (1996). *Wood-Destroying Insects–Wood Borers and Termites*, CSIRO Publishing, Collingwood, Victoria.

Creffield, J. W. (2005). "Call for the immediate declaration of all municipalities (metropolitan Melbourne and regional Victoria) as regions where homes, buildings and structures are subject to termite infestation," *Environmental Science*.

Darlington, J. P. E. C. (2000). "Termite nests in a mound field at Oleserewa, Kenya (Isoptera: Macrotermitinae," *Sociobiol*. 35, 25-34.

Diaz, M. J., Garcia, M. M., Eugenio, M. M., Tapias, R., Fernandez, M., and Lopez, F. (2007). "Variations in fiber length and some pulp chemical properties of Leucaena

varieties," *Indust. Crops Prod*. 26, 142-150. DOI: 10.1016/j.indcrop.2007.02.003

Donovan, S. E., Jones, D. T., Sands, W. A., and Eggleton, P. (2000). "Morphological phylogenetics of termites (Isoptera)," *Biol. J. Linn. Soc*. 70, 467-513. DOI: 10.1111/j.1095-8312.2000.tb01235.x

Elfaki, J. T., Gafer, M. O., Sulieman, M. M., and Ali, M. E. (2016). "Assessment of calcimetric and titrimetric methods for calcium carbonate estimation of five soil types in central Sudan," *Journal of Geoscience and Environment Protection* 4, 120-127. DOI: 10.4236/gep.2016.41014.

El-Nakhlawy, F. S. (2009). *Experimental Design and Analysis in Scientific Research*, Sci. Pub. Center, King Abdulaziz University, Jeddah, Saudi Arabia,

Eriksson, K. E L. (1993). "Concluding remarks: Where do we stand and where are we going?: Lignin biodegradation and practical utilization," *J. Biotechnol*. 30, 149-58. DOI: 10.1016/0168-1656(93)90036-m.

Fajar, A., Himmi, S. K., Adi, D. S., Tarmadi D., Nandika, D., Yusuf, S. (2020). "Examination of fecal pellet physical characteristics of an invasive drywood termite, *Cryptotermes dudleyi* (Isoptera: Kalotermitidae): A potential approach for species marker and non-destructive monitoring method." *IOP Conf. Ser.: Mater. Sci. Eng*. 935 012050. DOI: 10.1088/1757-899X/935/1/012050.

Gaudenzi, E. Cardone, F., Lu, X., and Canestrari, F. (2023). "The use of lignin for sustainable asphalt pavements: A literature review," *Construction and Building Materials* 362, article 129773. DOI: 10.1016/j.conbuildmat.2022.129773.

Gay, F. J. (1967). "A world review of introduced species of termites," C.S.I.R.0. Melbourne, Bull. No. 286, 88. https://portals.iucn.org/library/node/15469 (accessed on 06 June 2024).

Grassé, P., and Noirot, P. C. (1958). "Le meule des termites champignonnistes et sa signification symbiotique," *Ann. Sci. Nat., Zool. Biol. Anim*., 11, 113-28.

Guarino, V., Caus, F., and Ambrosio, L. (2007). "Porosity and mechanical properties relationship in PCL porous scaffolds," *J. Appl. Biomater. Biomech*. 5, 149-157.

Faragalla, A. A., and AL-Ghamdi, K. M. S. (1999). "Monitoring field populations of the harvester termite Anacanthotermes ochraceous (Burmeister) in two locations in western Saudi Arabia," *Sociobiol*. 34, 419-427.

Faragalla, A. A., Mohamed H., and Al Qhtani, M. H. (2013). "The urban termite fauna (Isoptera) of Jeddah City, Western Saudi Arabia," *Life Sci. J*. 10, 1695-1701.

FernandesIldeu, R. B. A., Emerson, A. C. J., Junior, S. R., and Mendonça, E. S. (2015). "Comparison of different methods for the determination of total organic carbon and humic substances in Brazilian soils," *Nutrição de Plantas Rev. Ceres*. 62, 496-501. DOI: 10.1590/0034-737X201562050011.

Hindi, S. S. (2011). "Evaluation of guaiacol and syringol emission upon wood pyrolysis for some fast-growing species," in: *International Conference on Environmental, Biological, and Ecological Sciences, and Engineering*, Paris.

Hindi, S. S., Bakhashwain, A. A., and El-Feel, A. A. (2011). "Physico-chemical characterization of some Saudi lignocellulosic natural resources and their suitability for fiber production," *JKAU; Met. Env. Arid Land Agric. Sci*. 21, 45-55.

Hindi, S. S., Abdel-Rahman, G. M., and AL-Qubaie, A. I. (2012). "Gross heat of combustion for some Saudi hardwoods," *Int. J. Sci. Eng. Investig*. 1, 10-14.

Hindi, S. S., and Abohassan, R. A. (2016). "Cellulosic microfibril and its embedding matrix within plant cell wall," *Int. J. Innov. Res. Sci. Eng. Technol*. 5, 2727-2734.

Hindi, S. S. (2017a). "Differentiation and synonyms standardization of amorphous and

crystalline cellulosic products," *Nanosci. Nanotechnol. Res*. 4, 73-85. DOI: 10.12691/nnr-4-3-1

Hindi, S. S. (2017 b). "Microcrystalline cellulose: The inexhaustible treasure for pharmaceutical industry," *Nanosci. Nanotechnol. Res*. 4, 22-31. DOI: 10.12691/nnr-4-1-3

Hindi, S. S. (2017 c). "Suitability of date palm leaflets for sulphated cellulose nano-crystals synthesis," *Nanosci. Nanotechnol. Res*. 4, 7-16. DOI: 10.12691/nnr-4-1-2

Hindi, S. S. (2017 d). "Nanocrystalline cellulose: Synthesis from pruning waste of *Ziziphus spina-christi* and characterization," *Nanosci. Nanotechnol. Res.* 4, 106-114. DOI: 10.12691/nnr-4-3-4

Hindi, S. S. (2017 e). "Some crystallographic properties of cellulose I as affected by cellulosic resource, smoothing, and computation methods," *Int. J. Innov. Res. Technol. Sci. Eng.* 6, 732-752. DOI: 10.15680/IJIRSET.2017.061127.

Hindi, S. S. (2017 f). "Some promising hardwoods for cellulose production: I. Chemical and anatomical features," *J. Nanosci. Nanotechnol. Res.* 4, 86-97. DOI: 10.12691/nnr-4-3-2

Hindi, S. S., and Abouhassan, R.A. (2018). "Method for making nanoocrystalline cellulose," U.S. Patent No. 10,144,786B2.

Hindi, S. S. (2020). "A method for converting micro- to nanocrystalline cellulose," U.S. Patent No. 10808045.

Hindi, S. S. (2021). "Nanocrystalline cellulose," U.S. Patent No. 11,161,918**.**

Hindi, S. S. (2022 a). "Urchin-shaped nanocrystalline material," U.S. Patent No. 11242410.

Hindi, S. S. (2022 b). "Sulfate-grafted nanocrystalline cellulose," U.S. Patent No. 11242411.

Hoogsteen, M. J. J., Lantinga, E. A., Bakker, E. J., Groot, J. C. J., and Tittonell, P. A. (2015). "Estimating soil organic carbon through loss on ignition: Effects of ignition conditions and structural water loss," *Eur. J. Soil Sci*. 66, 320-328. DOI: 10.1111/ejss.12224.

Huda, Md, Mousa, M., and Asiry, K. (2022). "Abundance and population dynamics of the key insect pests and agronomic traits of tomato (*Solanum lycopersicon* L.) varieties under different planting densities as a sustainable pest control method," *Horticulturae* 8, 976. 10.3390/horticulturae8100976

Hyodo, F., Inoue, T., Azuma, J., Tayasu, I., and Abe, I. T. (2000). "Role of the mutualistic fungus in lignin degradation in the fungus-growing termite," *Macrotermes gilvus* (Isoptera: Macrotermitinae)," *Soil Biol. Biochem.* 32, 653-658.

Ibrahim, A. K., Abubakar, T., Bappah, M., Muhammad, Z. (2022). "Soil, physical and chemical properties of termite mound and their adjacent soil". *Int. J. Agric. Rural Dev*. 25, A6450-6456.

Jost, C. (2020). "Nest-structure: Termites," in: *Encyclopedia of Social Insects*, C. K. Starr (ed.), Springer, Cham, Switzerland, pp. 651-660.

Keegstra, K., Talmadge, K. W., Bauer, W. D., and Albersheim, P. (1973). "The structure of plant cell walls: III. A model of the walls of suspension-cultured sycamore cells based on the interconnections of the macromolecular components," *Plant Physiol*. 51, 188-197. DOI: 10.1104/pp.51.1.188

King, H., Ocko, S., and Mahadevan, L. (2015). "Termite mounds harness diurnal temperature oscillations for ventilation," *Proc. Natl. Acad. Sci. USA.* 112, 11589-11593. DOI: 10.1073/pnas.1423242112

Klemm, D., Heublein, B., Fink, H. P., and Bohn, A. (2005). "Cellulose: Fascinating biopolymer and sustainable raw material," *Angew. Chem*. 44, 3358-3393. DOI: 10.1002/anie.200460587

Koehler, P. G., Short, D. E., and Kern, W. H. (1998). *Pests In and Around the Florida Home*, University of Florida Cooperative Extension Service, IFAS No SP 134. Gainesville FL.

Korb, J., and Linsenmair, K. (2000). "Thermoregulation of termite mounds: what role does ambient temperature and metabolism of the colony play?," *Insectes Soc*. 47, 357-363. DOI: 10.1007/PL00001731

Krishna, K. (1989). "Order Isóptera: Termites," in: *An Introduction to the Study of Insects* (6th Ed.), D. J. Borror, C. A. Triplehorn, and N. F. Johnson (Eds.), Saunders College Publishing, Philadelphia, PA, pp. 234-241.

Khristova, P., Kordsachia, O., and Khider, T. (2005). "Alkaline pulping with additives of date palm rachis and leaves from Sudan," *Bioresource Technol*. 96, 79-85. DOI: 10.1016/j.biortech.2003.05.005

Li, H., and Greening, C. (2022). "Termite-engineered microbial communities of termite nest structures: A new dimension to the extended phenotype," *FEMS Microbiol. Rev*. 46, fuac034.

Liu, X., Monger, H. C., and Whitford, W. G. (2007). "Calcium carbonate in termite galleries: biomineralization or upward transport?" *Biogeochemistry* 82(3), 241-50. http://www.jstor.org/stable/20456455.

Lopez, F., Garcia, M. M., Yanez, R., Tapias, R., Fernandez, M., and Diaz, M. J. (2008). "*Leucaena* species valoration for biomass and paper production in 1 and 2 year harvest," *Bioresource Technol.* 99, 4846-4853. DOI: 10.1016/j.biortech.2007.09.048.

Mahmood, S., Daur, I., Yasir, M., Waqas, M., and Hirt, H. (2022) "Synergistic practicing of rhizobacteria and silicon improve salt tolerance: Implications from boosted oxidative metabolism, nutrient uptake, growth and grain yield in mung bean," *Plants* (Basel). 11(15), article 1980. doi: 10.3390/plants11151980.

Neenan, M., and Steinbeck. (1979). "Calorific values for young sprouts in hardwood species," *Forest Sci*, 25, 455-461.

Ptáček, P., Brandštetr, J., Šoukal, F., and Opravil, T. (2013). "Investigation of subterranean termites nest material composition, structure and properties," Intech, Chapter 20, pp. 519-549. DOI: 10.5772/55145

Rasse, D. P., Dignac, M.-F., Bahri, H., Rumpel, C., Mariotti, A., and Chenu, C. (2006). "Lignin turnover in an agricultural field: From plant residues to soil-protected fractions," *Eur. J. Soil Sci*. 57, 530-538. DOI: 10.1111/j.1365-2389.2006.00806.x

Reginaldo, C., and Dianese, E. C. (2001). "The urban termite fauna of Brasilia, Brazil (Isoptera)," *Sociobiol*. 38, 323-326.

Rückamp, D., Martius, C., Bragança, M. A. L., and Amelung, W. (2011). "Lignin patterns in soil and termite nests of the Brazilian Cerrado," *Appl. Soil Ecol*. 48, 45-52. DOI: 10.1016/j.apsoil.2011.02.003.

Sharaf, M. R., Husain, M., Rasool, K. G., Tufail. M., and Aldawood, A. S. (2021). "Taxonomy and distribution of termite fauna (Isoptera) in Riyadh Province, the Kingdom of Saudi Arabia, with an updated list of termite species on the Arabian Peninsula," *Saudi J. Biol. Sci*. 28, 6795-6802. DOI: 10.1016/j.sjbs.2021.07.055

Shaikh, H. M., Anis, A., Poulose, A. M., Al-Zahrani, S. M., Madhar, N. A., Alhamidi, A., and Alam, M. A. (2021). "Isolation and characterization of alpha and nanocrystalline cellulose from date palm (*Phoenix dactylifera* L.) trunk mesh," *Polym*. 13, article

1893. DOI: 10.3390/polym13111893
Slaytor, M. (1992). "Cellulose digestion in termites and cockroaches: What role do symbionts play?," *Comp. Biochem. Physiol. B, Comp. Biochem.* 103, 775-784.
Su, N. Y., and Scheffrahn, R. H. (1998). "A review of subterranean termite control practices and prospects for integrated pest management programmes," *Integr. Pest Manag. Rev.* 3, 1-13. DOI: 10.1023/A:1009684821954
Trilokesh, C., and Uppuluri, K. B. (2019). "Isolation and characterization of cellulose nanocrystals from jackfruit peel," *Sci Rep*. 9(1), article 16709. DOI: 10.1038/s41598-019-53412-x
Tuomela, M., Vikman, M., Hatakka, A., and Itävaara, M. (2000). "Biodegradation of lignin in a compost environment: A review," *Bioresource Technol*. 72, 169-83.
Turner, J. S., and Soar, R. C. (2008). "Beyond biomimicry: What termites can tell us about realizing the living building?," in: *Proceedings of 1st International Conference on Industrialized, Intelligent Construction*.
Ulyshen, M. D. (2014). "Wood decomposition as influenced by invertebrates," *Biol. Rev*. 91, 70-85. DOI: 10.1111/brv.12158
Varma, A., Kolli, B. K., Paul, J., Saxena, S., and König, H. (1994). "Lignocellulose degradation by microorganisms from termite hills and termite guts: A survey on the present state of art," *FEMS Microbiol. Rev*. 15, 9-28. DOI: 10.1111/j.1574-6976.1994.tb00120.x
Wang, J. Y., Jamil, M., AlOtaibi, T. S., Abdelaziz, M. E., Ota, T., Ibrahim, O. H., Berqdar, L., Asami, T., Mousa, M. A. A., and Al-Babili, S. (2023). "*Zaxinone mimics* (MiZax) efficiently promote growth and production of potato and strawberry plants under desert climate conditions," *Sci. Rep.* 13, article 17438. DOI: 10.1038/s41598-023-42478-3
Wise, L. E., Merphy, M, M. D., and Adieco, M. (1946). "Chlorite holocellulose, its fractionation and bearing on summative wood analysis and on studies on the hemicelluloses," *Pap. Trade J*. 122, 35-43.
Wood, T. G., and Sands, W. A. (1978). "The role of termites in ecosystems," in: *Production Ecology of Ants and Termites*, M.V. Brain (ed.), Cambridge University Press Cambridge, UK, pp. 245-292.
Zachariah, N., Singh, S., Murthy, T., and Borges, R. (2020). "Bi-layered architecture facilitates high strength and ventilation in nest mounds of fungus-farming termites," *Scientific Reports* 10, article 13157.

Article submitted: October 21, 2024; Peer review completed: January 18, 2025; Revised version received: February 8, 2025; Accepted: April 10, 2025; Published: April 28, 2025.
DOI: 10.15376/biores.20.2.4495-4540

APPENDIX

Fig. A1. a) Termite life cycle, b) the workers within a living infected trunk of *Ziziphus spina-christi*, and c-g) mortar of the infected trunk

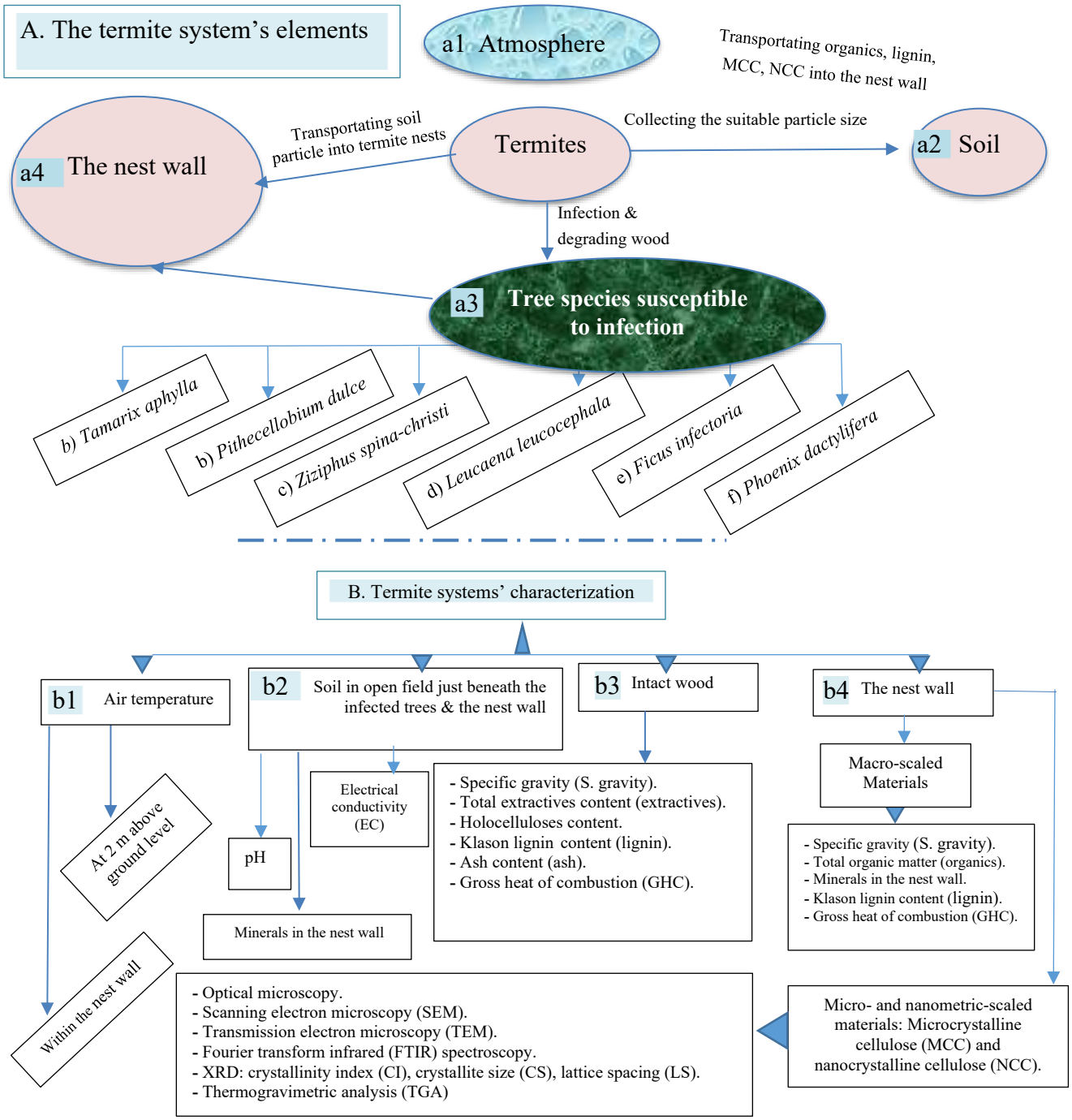

Fig. A2. The management plan for: (A) studying the termite system's elements: (a1) Air temperature, (a2) Soil, (a3) intact wood, (a4) t; (B) termite system's characterization: (b1) air temperature, (b2) soil in open field and the nest wall (b3) intact wood, (b4) nest wall.

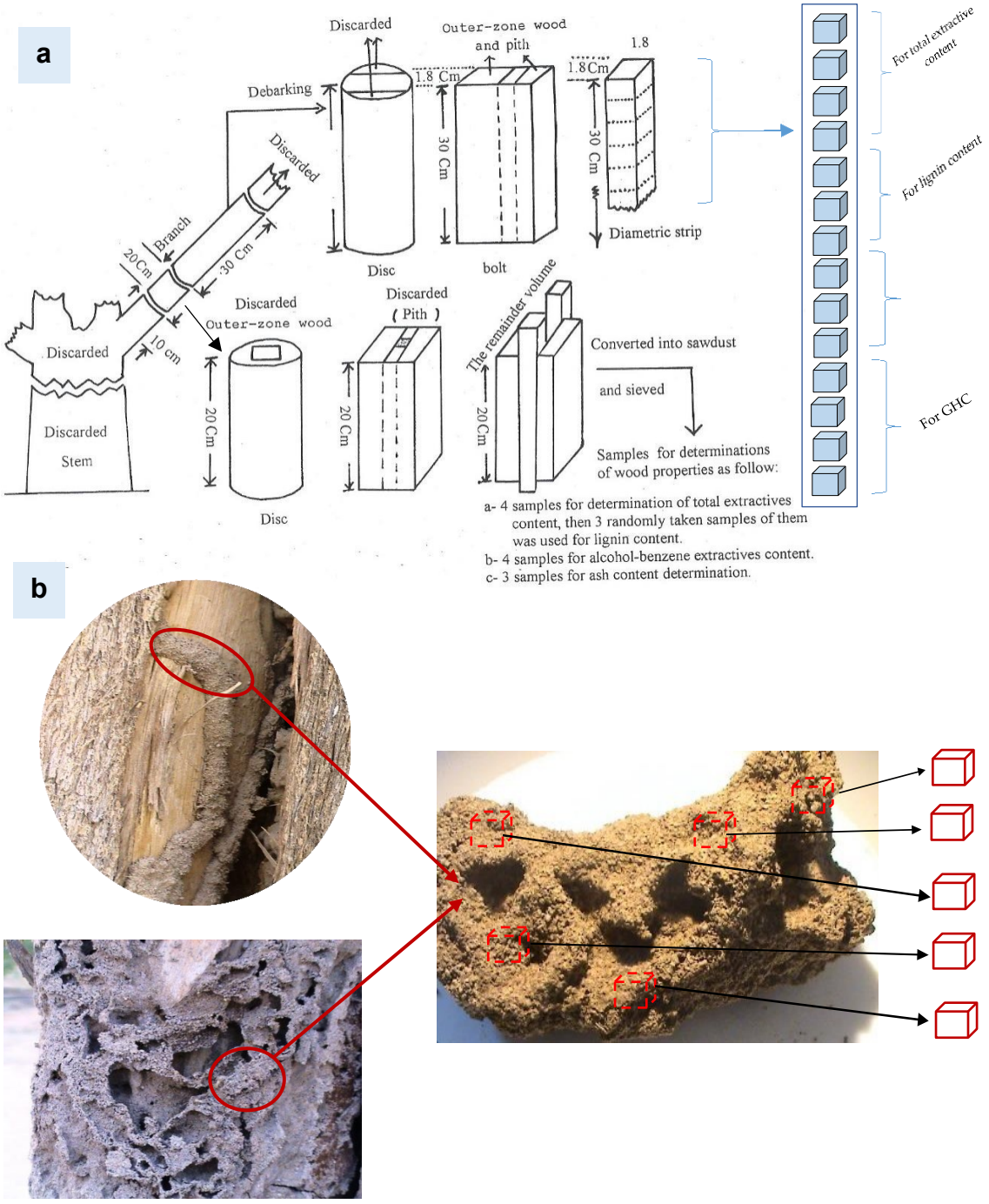

Fig. A3. Schematic representation of the procedure used for preparation of experimental samples: a) healthy wood (W_h), and b) nest wall of the six tree species.

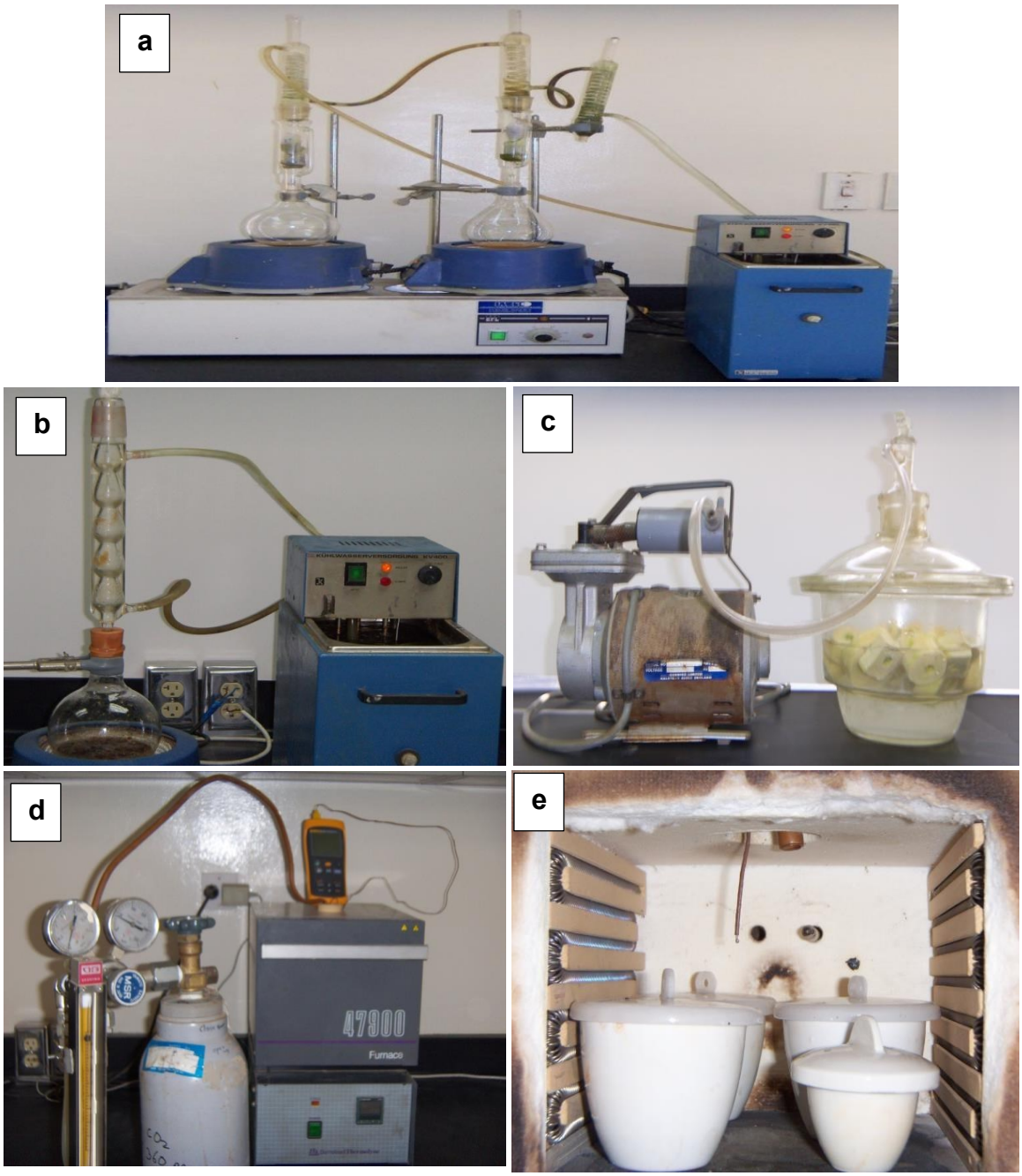

Fig. A4. Technical procedures, machinery and/or glassware used for characterization of the each of the healthy wood (W_h) and/or nest wall: a) Soxhlet apparatus for extracting total extractives content (TEC) and alcohol benzene extractives (ABE), b) Refluxed Pyrex apparatus for chemical separation of Klason lignin content (KLC), c) Vacuum pump-assisted water-saturation of the W_h, d) Electric muffle furnace used for determination of ash content of W_h, and e) Porcelain crucibles containing W_h samples to be ashed within the muffle furnace.

Table A1. Calculation of Different Chemical and Physical Properties of the Lignocellulosic Resources used for Construction of the Termite Nests Found at Hada Al-Sham, Saudi Arabia

Equation	Definitions
[1] $MC_{iw},\% = [(W_{adiw} - W_{odiw}) / W_{odiw}] \times 100$ [2] $MC_{nw},\% = [(W_{adnw} - W_{odnw}) / W_{odnw}] \times 100$ [3] $SG_{iw} = W_{odiw} / V_{siw}$ [4] $SG_{nw} = W_{odnw} / V_{odnw}$ [5] $Ash,\% = (W_{aiw} / W_{efiw}) \times 100$ [6] $Extractives,\% = [(W_{odiw} - W_{efiw}) / W_{odiw}] \times 100$ [7] Holocelluloses [8] $Lignin,\% = (W_{lr} / W_{efiw}) \times 100$ [9] $Organics\ in\ virgin\ soil,\% = [(W_{vs} - W_{ttvs}) / W_{vs}] \times 100$ [10] $Organics\ in\ nest\ wall,\% = [(W_{nw} - W_{ttnw}) / W_{vs}] \times 100$ [11] $GHC,\ calories/g = [(t\ E_e) - e_1 - e_2 - e_3] / W_{odiw}$ or W_{odnm} [12] $t = t_c - t_a - r_1\ (b-a) - r_2\ (c-b)$ [13] $e_1 = = c_1$ if 0.0709N alkali was used for the titration. [14] $e_2 = (13.7 \times c_2)(W_{odiw}$ or $W_{odnm})$ [15] $e_3 = 2.3 \times c_3$ [16] $r_1 = (T_a - T_b) / 5$, calories/min. [17] $r_2 = (T_d - T_e) / 5\}$, calories/min.	W_{adiw}: Weight of air-dried intact wood, g. W_{odiw}: Weight of oven-dried intact wood, g. W_{adnw}: Weight of air-dried nest wall, g. W_{odnw}: Weight of oven-dried nest wall, g. V_{siw} = Volume of water-saturated intact wood, cm^3. V_{odnw}: Volume of oven-dried nest wall, cm^3. W_{aiw}: Weight of ash matter of intact wood. W_{efiw} = Weight of extractive-free oven-dried intact wood meal, g. W_{lr}: Weight of lignin residues, g. W_{vs}: Weight of virgin soil sample (open field), g. W_{ttvs}: Weight of the thermally-treated virgin soil sample (open field), g. W_{nw}: Weight of nest wall sample, g. W_{ttnw}: Weight of the thermally-treated virgin soil sample (open field), g. GHC: Gross heat of combustion, calorie/g = Energy equivalent of the calorimeter, determined under standardization e_1: Thermochemical correction in calories for heat of formation of nitric acid (HNO_3). e_2: H_2SO_4. e_3: Thermochemical correction in calories for heat of combustion of fuse wire. a: Time of combusting the sample. b: Time (to nearest 0.1 min.) when the temperature reaches 60% of the total rise in temperature. c: Time at beginning of the post-period, whereby the rate of temperature change has become constant. c_1: milliliters of standard alkali solution used in the acid titration c_2: sulfur content in the sample,%. c_3: centimeters of fuse wire consumed in firing. T_a: Temperature at time of combusting the sample T_b: Temperature at time of combusting the sample. T_c: Temperature at the point c (See the temperature rise curve, at the left side◦◦). T_d: Initial temperature at the final period after combusting the sample.

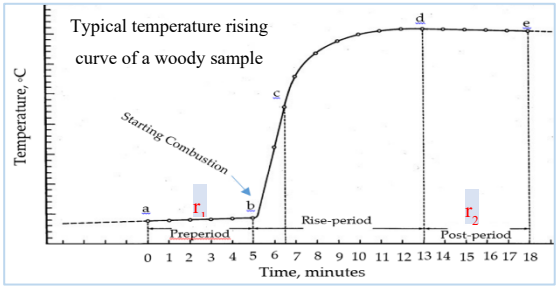

T_e: Final temperature at the last period after combusting the sample.

r_1: rate (temperature units per min) at which the temperature was rising during the 5-min. period before combusting the sample.

r_2: rate (temperature units per min) at which the temperature was rising during the 5-min. period after time, where r_1 and/or r_2 = '+' when the temperature is rising and '-'when the temperature is falling.

[18] $C_s = K\lambda/\beta_{1/2}\text{Cos }\theta$ [19] $L_s = n\lambda / 2\sin\theta$	K: The correction factor and usually taken to be 0.91 λ: The radiation wavelength of X-rays incident on the crystal (0.1542 nm). θ: The diffraction angle. $\beta_{1/2}$: The corrected angular full width at FWHM. FWHM: The full width at half maximum of a XRD- peak. n: An ordinal number taking a value of "1" for diffractograms having the strongest intensity.
[20] Compression strength = F_f/A [21] MoE = Stress/Strain at the PL = σ/ε [22] $\varepsilon = [\Delta L/L_o] = [(Lf - L_o)/L_o]$ [23] $EaF = \Delta Lf = [(Lf - L_o)/L_o] \times 100$	F_f: Force at failure in Newton (N).
	A: Cross-section area (m^2) of the nest wall.
	σ: Compression stress (Pa).
	L_f: The length of the nest wall at failure.
	L_o: The initial length of the nest wall at failure.
[24] $d = W_{odnw} / V_{odnw}$ [25] $P = 1 - (d/d_p)$	d_p: Density of non-porous material.

[1] Moisture content of intact wood; [2] Moisture content of nest wall; [3] Specific gravity of intact wood; [4] Specific gravity of nest wall; [5] Ash content (ash) of intact wood; [6] Total extractives content (extractives) of intact wood; [7] Holocelluloses content of intact wood; [8] Klason lignin (lignin) content of intact wood; [9] Total organic matter (organics) in virgin soil; [10] Total organic matter (organics) in nest wall; [11] Gross heat of combustion of intact wood; [12] Temperature rise; [13] Correction for heat of formation of nitric acid; [14] Correction for heat of formation of sulfuric acid; [15] Correction for heat of formation of the nickel chromium-fuse wire; [16] Temperature rate for pre-period of combustion; [17] Temperature rate for post-period of combustion; [18] Crystallite size, nm using Scherer equation with respect to the crystallographic plane (CP) of '002'; [19] Lattice spacing, nm using the Bragg's equation at CP of 002; [20] Tensile strength (MPa), [21] Modulus of elasticity (GPa), [22] Tensile strain, [23] Elongation at failure (%); [24] Real density of the nest wall; [25] Porosity.

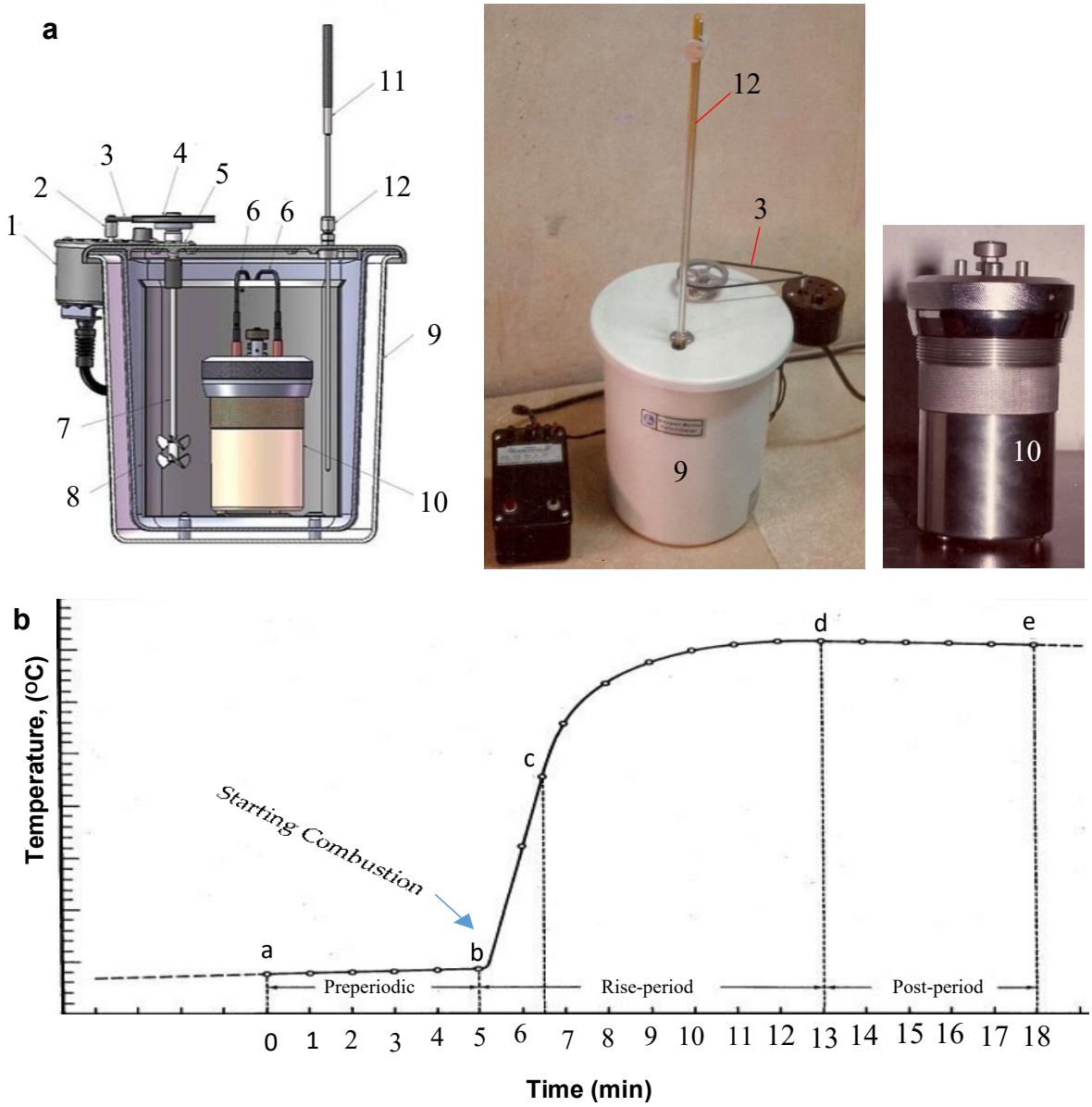

Fig. A5. Gross heat of combustion determination (GHC): a) Parts of the oxygen bomb calorimeter used for measuring GHC of the healthy wood and the nest wall, and b) Typical temperature rising curve of a woody sample